A Hydrogel Microneedle-Assisted Assay Integrating Aptamer Probes and Fluorescence Detection for Reagentless Biomarker Quantification

by

Hanjia Zheng

A thesis
presented to the University of Waterloo
in fulfillment of the
thesis requirement for the degree of
Master of Applied Science
in
Electrical and Computer Engineering (Nanotechnology)

Waterloo, Ontario, Canada, 2022

© Hanjia Zheng 2022

Author's Declaration

This thesis consists of material all of which I authored or co-authored: see Statement of Contributions included in the thesis. This is a true copy of the thesis, including any required final revisions, as accepted by my examiners.

I understand that my thesis may be made electronically available to the public.

Statement of Contributions

Hanjia Zheng was the sole author for Chapters 1, 2, 3 and 5 which were written under the supervision of Dr. Mahla Poudineh and Dr. Amin GhavamiNejad.

This thesis consists in part of a manuscripts written for publication. This manuscript has been submitted for reviewing. Exceptions to sole authorship of material are as follows:

Research presented in Chapters 2, 3, 4 and 5:

Dr. Amin GhavamiNejad is the co-authors on any publications relating to this work.

The animal experiment in Chapter 4 was conducted at the University of Toronto by Hanjia Zheng and Amin GhavamiNejad under the supervision of Dr. Mahla Poudineh and Dr. Adria Giacca.

Citations: Zheng, Hanjia, Amin GhavamiNejad, Peyman Ghavami Nejad, Melisa Samarikhalaj, Adria Giacca, and Mahla Poudineh. "A Hydrogel Microneedle-assisted Assay Integrating Aptamer Probes and Fluorescence Detection for Reagentless Biomarker Quantification." *bioRxiv* (2021).

As lead author of these chapters, I was responsible for contributing to conceptualizing study design, carrying out data collection and analysis, and drafting and submitting manuscripts. My coauthors provided guidance during each step of the research and provided feedback on draft manuscripts.

Abstract

Point-of-care (POC) transdermal biosensors targeting skin interstitial fluid (ISF) catch rising attention during the recent decade. Typical skin ISF sampling manner includes suction blisters, microdialysis, reverse iontophoresis and microneedles. In this case, analyzing ISF via microneedle devices enables patient health monitoring as a minimally invasive, pain-free, easy-to-use and cost-effective manner. However, most MN-based diagnostic approaches require complicated fabrication processes or post-processing of the extracted ISF. Here we show on-needle measurement of target analytes by integrating hydrogel microneedles (HMN) with aptamer probes as the target recognition elements. Fluorescently tagged aptamer probes are covalently attached to the methacrylated hyaluronic acid (MeHA) hydrogel matrix while a crosslinked patch is formed by UV irradiation. Such a target sensing manner enables rapid (2 min) measurement of glucose, adenosine triphosphate, L-tyrosinamide, and thrombin under real skin environment. The system enables the specific and sensitive quantification of rising and falling concentrations of glucose in an animal model of diabetes to track hypoglycemia, euglycemia, and hyperglycemia conditions. The assay enables rapid and reagentless target detection and can be readily modified to measure a wide range of target analytes *in vivo*. Our system has the potential to improve the quality of life of patients who are in need of close monitoring of biomarkers of health and disease.

Acknowledgements

Dedication

This thesis is dedicated to the memory of my grandmother Jifang and Xiulan. Your love and trust inspire me spiritually throughout my life.

Table of Contents

List of Figures

List of Tables

Chapter 1
Background

This chapter brings a brief introduction to point-of-care diagnostic device and transdermal biosensor, especially microneedle-based biosensor, indicating the importance and potential of applying microneedle in POC transdermal biosensor. Additionally, types of microneedles and their sampling manner, advantages and main obstacle are listed.

1.1 Point-of-care (POC) transdermal biosensor and skin interstitial fluid

Nowadays, point-of-care (POC) diagnostic plays an essential role in the medical assisting system for disease diagnosis, monitoring and management. POC, a type of rapid or continuous, easy-to-use, cost-effective medical diagnostic manner performed at or near the patient, catches rising attention recently, specifically after the COVID-19 pandemic[1]. Typical POC includes blood glucose testing[2], blood gas monitoring[3], human chorionic gonadotropin (HCG) pregnancy testing[4], drug abuse screening[5] and rapid cardiac markers testing[6]. Those techniques have been widely applied in clinical usage, which can help the patients, health care and doctor sufficiently track patients' health condition to provide rapid and proper diagnosis[7]. In addition, some of POC devices with cost-effective test strips do not require pre-trained personnel, such as glucose meter and HCG test strip[2,4]. During the COVID-19 pandemic, the utilization of rapid antigen test kit significantly decreases the likelihood of cross infection and alleviates the overload of medical system[1]. Currently, developers pay more attention to the POC devices for infectious and chronic disease detection[2,8,9].

Biosensor system consists of a bioreceptor, a transduction element and electronic circuit including a signal amplifier, a processor, and a display unit[10,11]. Bioreceptor is also known as biological recognition element, which is biological component that can specifically interact with the target analytes[10,11]. Common bioreceptor includes enzymes, antibody, hormone, and nucleotides[11]. Transducer is a physical component that can amplify the biochemical signals generated by bioreceptor,

then transduce them in the form of electrical, optic, or piezoelectric signal[10,11]. Eventually, the transduced signal will be amplified, processed, and displayed as digital data by electrical circuit[10,11].

Transdermal biosensor is a self-contained integrated device to collect skin interstitial fluid (ISF) and provide quantitative or semi-quantitative analytical information for single or multiple metabolites with high selectivity and specificity[12–14]. ISF is the main component of body fluid surrounding the cells and blood vessels throughout all the tissues, acting as a reservoir holding the waste product generated by cells, and nutrients diffused from plasma[15]. ISF constitutes 97% of extracellular fluid, which makes it a major part of internal environment[15,16]. Therefore, ISF is considered as the mixture of serum and cellular materials, which is an essential source of comprehensive biomarkers including macromolecules (*e.g.*, protein, DNA and RNA), metabolites (*e.g.,* glucose, cortisol, and Adenosine 5'-triphosphate (ATP)), electrons and drugs (*e.g.,* antibiotics and heroin)[14,17–20]. In addition, biomarkers existed in skin ISF and blood shares high similarity[14,15,21]. For instance, 83% of proteins exists in blood serum can also be detected in ISF[21]. Moreover, some biomarkers, such as exosome and adaptive immune cells, are exclusively existed in skin ISF. According to Kool et al., roughly 50% of proteins in ISF cannot be detected in blood[22]. Beside the great biomarker diversity, ISF is a long-term, stable, and continuous sample source due to the lack of clotting factors[15]. Therefore, it is considered as an excellent sample source for long-term real-time biosensing sensing.

Although skin ISF shows obvious superiority in various aspects, skin ISF is hard to collect. Common ISF sampling manner includes biopsy, suction blisters, microdialysis, reverse iontophoresis and most recently, microneedle (MN)[18,22,23]. Over 70% of skin ISF located in dermis layer, can only be collected by biopsy, which leads to tissue damage and intracellular fluid contamination[23]. Alternatively, suction blisters and microndialysis ISF sampling manner is less painful, but still requires a long sampling time, medical expertise, and even local anesthesia[18,22,23]. Reverse iontophoresis utilizing electric current to extract specific ISF component (*e.g.,* glucose) is also an alternative[23]. However, this

manner can only collect limited types of small molecules, and a calibration ahead of detection is required[23]. Overall, the ISF sampling manners mentioned above are time-consuming, non-portable and highly invasive. Therefore, difficulty in ISF sampling hinders the utilization of ISF as a source to sample biomarkers. Ideally, a great ISF sampling manner should rapidly extract 1 to 10 μL of ISF without causing tissue damage or even uncomfortable feeling to the patients[14,15,19,23]. In addition, the sampling process should be simple and user-friendly, which allows for patients' self-administration[14,15,19,24]. A novel skin ISF sampling approach, microneedle (MN) meeting all the criteria mentioned above, has become a research hotspot recently[14,15,19,24–26]. It opens a new avenue for transdermal biosensor development with its pain-free and easy-to-use features.

Currently, transdermal biosensors, such as Dexcom G6[27], Enlite Sensor (Guardian REAL-Time System)[28], and Abbott FreeStyle Libre[29], have been successfully commercialized, especially in the POC glucose sensing market. However, the market of MN-based biosensor, which has great potential to be expanded in the future, still vacancies. More MN based biosensor with great commercialization potential should be developed. In this paper, I will provide an overview of the MN-based transdermal biosensor, followed with introducing and characterizing our novel hydrogel MN-based biosensor integrating aptamer probes for biomarker detection.

1.2 MN-based ISF sampling technique

MN-based biosensor is a pain-free, minimal invasive, easy-to-use transdermal sensing device with an array of miniaturized needles down to the micrometer scale, which its primary function is to penetrate through skin to access skin ISF without touching blood vessels and nerve ends[14,15,21]. Compared with conventional needle-based blood collection, MN-based ISF sampling shows advantage from various aspects.

First, according to Liu et al., the improper waste management and sterilization of used hypodermic needles may increase the risk of blood borne infections (*e.g.,* HIV, HBV and HCV) spreading[21]. In addition, blood collection using hypodermic needle requires skilled personnel for sample collection, waste management and needles recycling, which is impossible for self-administration[21]. However, user friendly and simple-to-dispose MN-based ISF sampling device is safe for patients to perform the test independently[21]. Moreover, microneedle devices enabling both continuous target detection and drug delivery, also known as self-regulated administration device, can provide rapid and appropriate treatment based on patients' health condition[21].

Second, skin ISF is easy and safe to access compared with blood[14,15,21,23]. Anatomically, human skin is composed of two layers: epidermis and dermis[21]. Epidermis is the out most layer of human skin as the protective barrier between human body and environment, which consists of multiple types of specialized cells and inflammatory cells with a total thickness of 10-200 μm[30]. Dermis is the inner layer of human skin, where the blood vessels, nerves, lymphatic vessels, and hair follicles located[30]. Typical MN devices with a needle length of $200 - 1500$ μm access skin ISF located in dermis layer where is absence of blood vessels and nerve ends[14,21]. However, blood vessels and other types of ISF are deeply located in the dermis layer, where is enrich of nerve ends, lymphatics, and glands[14,21]. Therefore, utilizing MN devices for ISF sampling could significantly lower the risk of inflammation response and tissue damage due to improper operation[14,15,21]. Overall, MN device is an easy-to-use, minimally invasive, pain-free, safe ISF sampling manner, thus, has great potential to be applied in POC transdermal sensing platform.

MN-based ISF sampling principle is determined by the structure and material of MN devices. Generally, MNs can be classified as hollow MNs, porous MNs and hydrogel MNs.
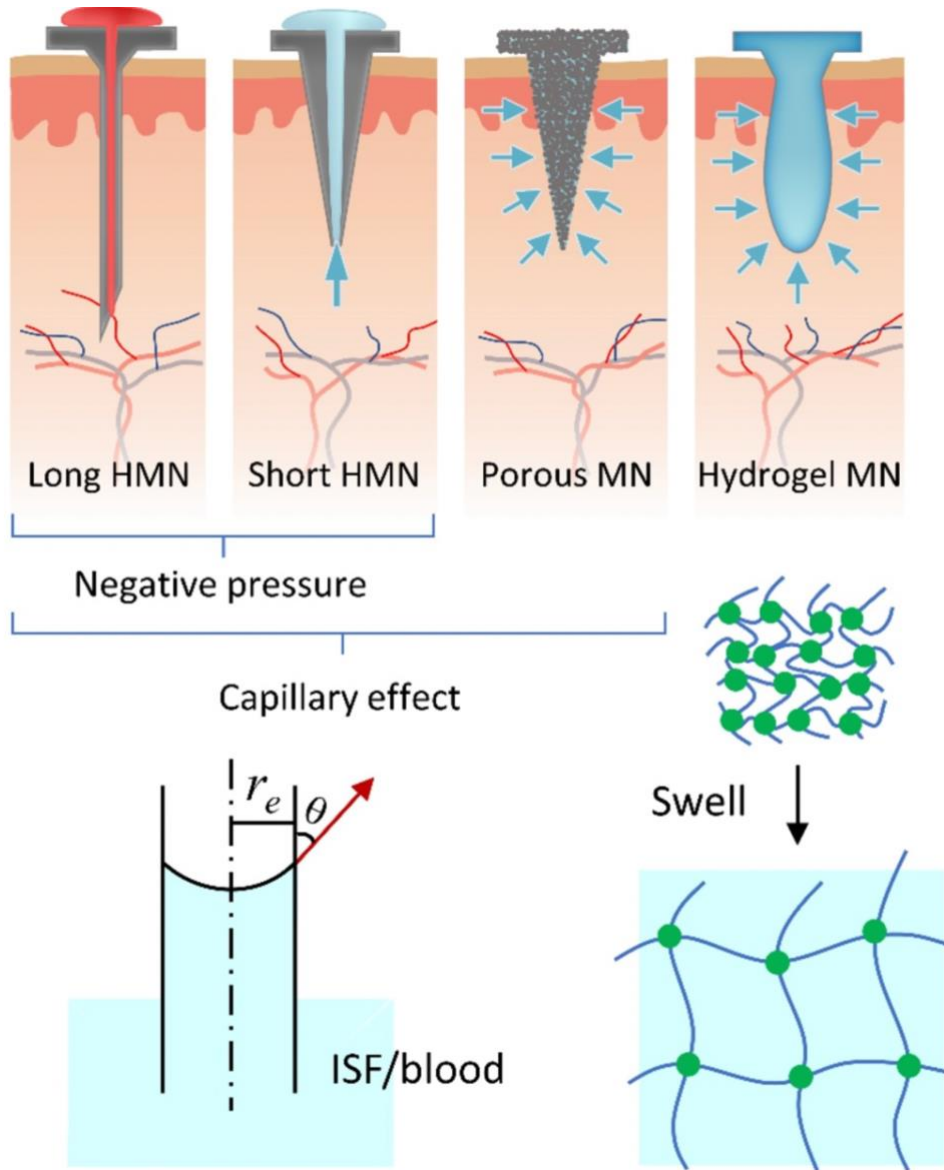
Figure 1.1 Schematic of MN ISF sampling strategy. Differently shaped and structural MNs for transdermal biofluid sampling driven by negative pressure, capillarity, or swelling[21].

Hollow MNs commonly constructed from silicon or metal, contains a long, thin tubular inside the needle, which helps to generate a self-powered capillary structure[19,21]. Skin ISF could be extracted based on the negative pressure generated by capillary force[15,19,21]. Typically, hollow MNs for skin ISF sampling is also known as short hollow MNs, which needle length is less than 900 μm[21]. According to

Miller et al., hollow MNs could start ISF collection after 30-120 s skin insertion, then yield 1.51 μL of skin ISF with 10-15 min sampling time. The main obstacles with hollow MN applications are the complex fabrication protocols and the potential risk of MN clogging[31]. In addition, the complex and time-consuming fabrication process, and low sampling volume are main obstacles in hollow MNs.

Similar to hollow MNs, porous MNs also rely on negative pressure generated by their internal capillary structure[21,32]. Different from the single capillary channel in hollow MNs, porous MNs are fabricated with an internal high-density capillary network, which can extract skin ISF more sufficiently[21,32,33]. According to Wang et al., porous MNs with needle length of 700-1500 μm could extract 1-10 μL of skin ISF after $2 - 10$ min skin insertion[14]. Theoretically, porous MNs' ISF extraction capability mainly depends on their material, pore size and needle length. According to Liu et al., porous MNs are manufactured with polymer (*e.g.,* Polydimethylsiloxane (PDMS) and polyvinyl alcohol (PVA)), and mental[21]. Although porous MNs has greater ISF sampling capability, the fabrication process is still complex and dangerous since multiple hazardous chemicals (e.g., Hydrofluoric Acid (HF)) are involved[33].

Hydrogel microneedles (HMNs) is a unique ISF sampling manner, which relies on osmotic pressure generated by fluid diffusion and material absorption capability[17,21,26,34,35]. Therefore, ISF sampling efficiency of HMNs is determined by its fabrication hydrogel polymer, such as polystyrene, polycarbonate, PVA, gelatin, hyaluronic acid (HA) and poly(ethyleneglycol)[17,21,24,26,36]. Such materials form a crosslinked polymer chain network enrich with hydrophilic groups after heating or UV exposure[17,21,24]. The crosslinked polymer network could continuously absorb ISF to get swelled, until the swelling force and elastic network retraction force reach balance[21]. With the discovery of hydrogel polymer material, HMNs' ISF adsorption capability has been significantly improved during recent years. Date back to 2014, a HMNs composed of poly(methyl vinyl ether-alt-maleic acid) and poly(ethylene glycol) could extract 0.84 μL of ISF sample from porcine skin in 1 h[37]. Yet, in 2020, He

et al. demonstrated the HMN-based metabolites sensor fabricated with PVA and chondroitin sulfate (CS) which could achieve 7 μL ISF within 6 min for *in vitro* experiment[38]. In the same year, a MN fabricated with multipolymeric hydrogel consisting of poly(potassium acrylate coacrylic acid) (PKAAA), poly(acrylic acid) and poly(methylvinylether comaleic acid) was reported, which is able to absorb up to 6 μL ISF within 10 min during *in vivo* experiment[39].

The crosslinked polymer network of HMNs is not only responsible for the excellent ISF sampling capability, but also helpful for sample recovery for downstream processing[21,24]. Centrifugation and solvent extraction are two common simple and rapid ISF recovery strategy[21,24]. Chang and his colleges successfully recovered glucose and cortisol from swelled methacrylated hyaluronic acid (MeHA) HMNs by 10 min centrifugation, followed with target quantification using glucose and cortisol assay kit[24]. In 2020, He et al. reported a heat triggered dissolvable HMNs composed of PVA and CS which remains insoluble under room temperature but dissolve rapidly with heat treatment over 60 ℃ [38]. The collected analytes including electrolyte ions, glucose, lactate, and protein could be quantified directly after HMNs was dissolved and the result is reliable[38]. In addition, compared with other types of MN-based ISF sampling device, most HMNs devices are made up with biocompatible material though a simple fabrication process[17,24,26,36–39].

Overall, HMNs provides a sufficient, safe, and rapid ISF sampling technique, which has great potential to be combined with biosensor. According to Kim et al., MN-based biosensors can offer continuous measurement and real-time monitoring for specific analytes with high accuracy[40]. In the next section, I will introduce the common MN-based biosensor integration strategies, followed with the analysis and evaluation of some current MN-based biosensors.

1.3 MN-based biosensors

Integrating biosensors on MNs enabling in-situ ISF characterization has become a research hot spot for the past decade due to its pain-free, easy-to-use and short response time features[14,24]. With the development of complementary sensing techniques, MN-based biosensing strategy has been established[2]. MN-based biosensing strategies consist of two major components, off device and on device strategy[21].

"Off device" strategy mainly describe the MN biosensors utilize MN as a ISF sampling device only[21]. The extracted ISF needs to be collected or recovered for subsequent specific biomarker detection[21]. This approach usually limits the target detection range or complicates the detection process. In this case, the target detection range and detection process are mainly determined by the subsequent target detection assay, instead of the MN device[24]. In addition, the extracted ISF will be diluted during the recovery process, biomarkers with low initial concentration (*e.g.,* miRNA) will fall out of the detection range[21,24]. For instance, Zhu et al. demonstrated a gelatin methacryloyl (GelMA) HMN utilizing off device strategy for glucose quantification (see Table 1). Although the glucose detection range is appropriate (50 to 600 mg dL^{-1}), the detection process after glucose recovery is complex and time-consuming (130 min)[17]. Overall, off device is the original sensing strategy, but its target detection range is restricted by the target detection assay and target's initial concentration.

Oppositely, "on device" MN-based sensing strategy avoids the target recovery process but perform the target detection assay on the MN patch by the integrated bioreceptor or electronic circuit[21]. Compared with off device MN biosensor, on device MN biosensor showed superiority on the shorter detection time and more comprehensive generalization potential[15,21].

Electrochemical MN biosensor is one of the common on device sensing strategies, which consists of sensing materials (enzyme or nucleic acid) and conductive MN patch[21,40,41]. As indicated in figure 1.2, enzyme-based MN biosensor measures target concentration through current variation

generated during enzyme-catalyzed reaction of target[21,41]. In this case, the current variation is proportional to the target concentration. Meanwhile, to avoid the intrinsic influence due to the elevated operating volage caused by the dissolved oxygen in skin environment, a redox mediator is involved to transfer the electrons generated from enzyme to the electrode[21,42].
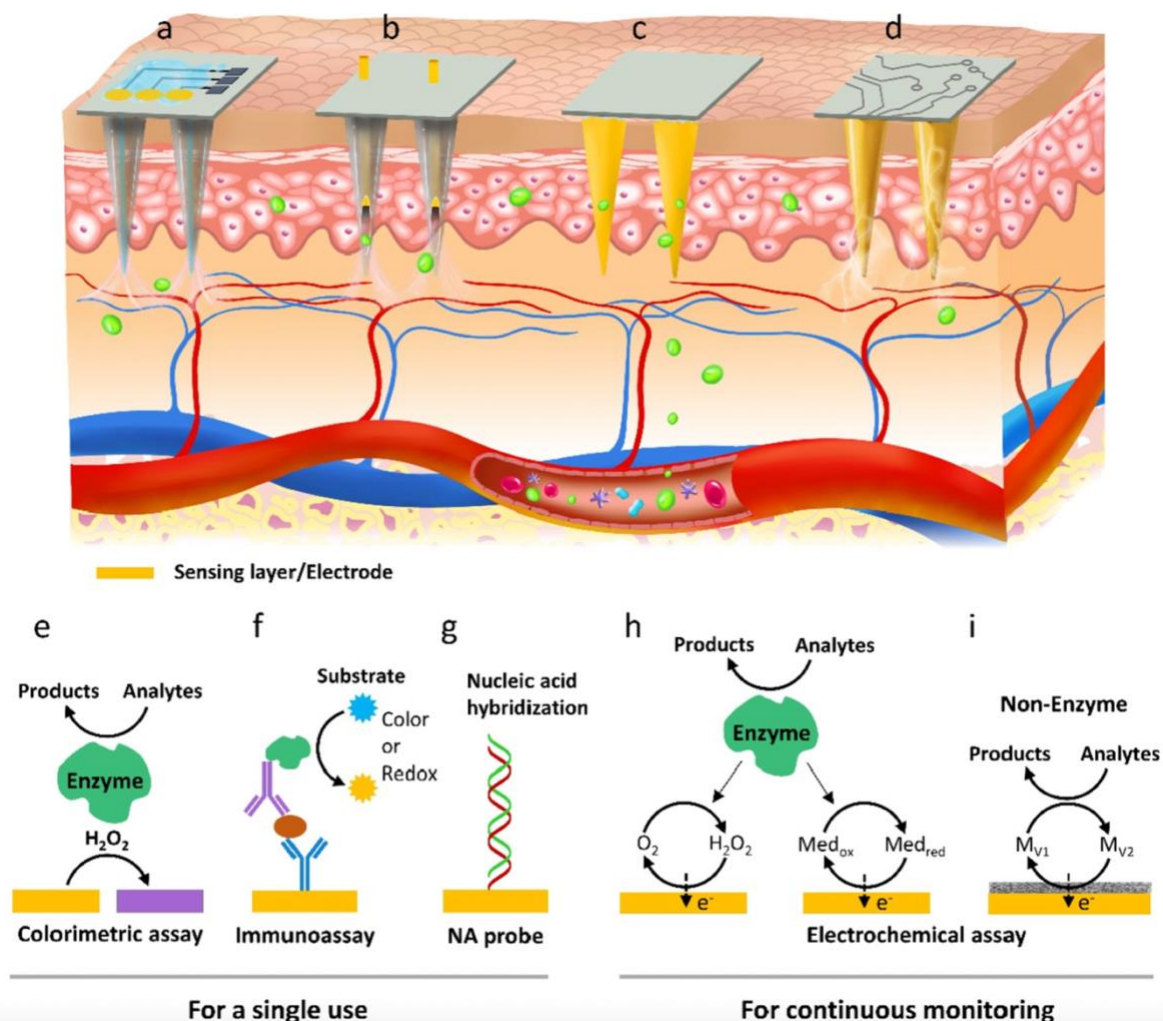
Figure 1.2 Schematic of four types of typical MN-based biosensing strategy. **a,** hollow MN interpolated with specific sensor and **b,** electrochemical electrode, **c,** surface functionalized and **d,** metalized MNs. **e–i,** indicate the common sensing mechanisms of different MN sensors: colorimetry, immunoassay, nucleic acid recognition, and electrochemistry.

Another popular type of MN-based biosensor is the MN integrated with bioreceptor. A wide range of bioreceptor and signal can be integrated with on device MN biosensor, which gives rapid and reliable detection results[21]. Shown in figure 1.2, typical bioreceptors, such as enzyme, antibody and

9

nucleic acid probe, decorated MN biosensor enables the target quantification by measuring the colorimetric, fluorescent, or electrochemical signal generated from colorimetric assay, enzyme-linked immunosorbent assay (ELISA) or nucleic acid hybridization[21]. In 2019, a poly(ethylene glycol) diacrylate (PEGDA) MN encapsuled with photonic crystal (PhC) barcode was reported for multiple types of inflammatory cytokine (TNF-α, IL-1β, and IL-6) detection[25]. The target specific antibody barcodes with certain structural color were designed for each cytokine and embedded into MN patch during fabrication process[25]. During ISF sampling process, the antibody immobilized in the barcode would capture the corresponding cytokine, followed with the binding of detection antibody, generating strong fluorescent signal proportional to target concentration[25]. In 2021, a polystyrene MN-based biosensor for ultrasensitive and quantitative protein detection was demonstrated[43]. With antibody immobilized on the needle surface, this device can specifically capture the target protein during ISF sampling process, followed with an on-needle fluorophore-linked immunosorbent assay (FLISA) for generating strong fluorescent signal[43]. According to Wang et al., this device was able to measure the concertation of cocaine antibody, Interleukin-6 (IL-6) and periostin with high accuracy and specificity[43]. An aptamer probe decorated porous MN based biosensor was also demonstrated for endotoxin detection utilizing fluorescent signal[33]. Aptamer probe is a short single stranded DNA or RNA molecule that can bind to certain target with high specificity and affinity[33]. In this case, aptamers immobilized on MN enables target capturing during ISF sampling process[33]. Subsequently, the MN was incubated with fluorophore labeled aptamer to form the aptamer-target-aptamer complex[33].

Considering all the MN-based sensing devices mentioned above, although the ISF sampling time is shorten and target recovery process is avoided, the subsequent target detection process is still complex and time consuming, which results in an overall long response time (see **Table 1.1**). Compared with the other MN-based biosensor, the total response time of aptamer decorated MN array is relatively shorter, even with the longest ISF sampling time (60 min). This effective target detection process is

10

mainly due to aptamer's rapid target capturing feature. In conclusion, on device MN-based sensing strategy enables accurate and pain-free target detection, but the subsequent time-consuming detecting procedure significantly limits its application in commercialized transdermal biosensor. However, the relatively shorter response time and excellent target detection accuracy of aptamer decorated MN array inspire a new avenue of on device MN-based biosensor development. In the next part, the definition of aptamer and its application in biosensor will be introduced.

Table 1.1 Comparison of response time of different MN-based sensors.

Device	Capture	Washing	Blocking	Detection	Washing	Total time
GelMA MN[17]	10 min	5 min for target recovery	-	120 min with glucose assay kit	-	130 min
FLISA[43]	30 s-20 min	10 min	30 min	120 min incubation with Ab + 30 min incubation with plasmonic fluor	10 min	200 min-220 min
Aptamer decorated MN array[33]	60 min	10 min	-	60 min incubation with FAM labeled aptamer	10 min	140 min
Encoded MNs[25]	40 min	10 min	-	120 min incubation with detection Ab	10 min	180 min

1.4 Aptamer probes for target recognition

As mentioned in the last section, aptamer is a short, single stranded DNA, RNA or polypeptide probe, which exhibit high binding affinity and excellent target recognition specificity and sensitivity for its corresponding target[44,45]. In this paper, we focus on the nucleic acid aptamer, especially DNA aptamer.

A wide range of analytes can be detected by DNA aptamer, including heavy metal ions, metabolites (e.g., glucose, cortisol, and ATP), drugs and toxins (e.g., vancomycin and endotoxin), proteins (e.g., thrombin and insulin), and even cells (e.g., bacteria and immune cells)[45]. The aptamer - ligand interaction is configured through van del waals force, electrostatic interactions, pi-pi stacking, hydrogen bond and hydrophobic interactions[45]. In this case, aptamer-ligand complex is strong enough to remains stable even with the presence of aptamer's complementary strand[44,45]. Some aptamer-ligand binding changes aptamer's conformation, which would influent the target binding affinity[44,45].

Compared with antibody, modification available for DNA aptamer is more abundant, which allows for more immobilization and signal transducing strategies[45]. In addition, DNA aptamer with a length of 20 to 60 nucleotides is easy to obtain due to the simple synthesis and purification procedure[45]. In addition, as mentioned above, aptamer mediated target detection significantly reduces the processing time by avoiding multiple washing and incubation steps.

Tang et al. exhibited aptamer switch probes with a strand displacement strategy[44]. Briefly, the Cy3 fluorophore-conjugated aptamers hybridized with a DNA competitor strand that has been conjugated to a quencher (Dabcyl) molecule, called the quencher strand, forming an aptamer-quencher complex[44]. The aptamer-quencher complex retains the fluorophore and quencher in proximity, producing no signal in the absence of a specific target[44]. When the aptamer binds to the target, the quencher competitor strand dissociates and alleviates quenching of the fluorophore, producing a signal without requiring for any post-processing steps such as washing or adding a detection reagent[44].

In conclusion, aptamer mediated biosensor exhibits greater potential to be applied in biosensing platform due to its easy-to-synthesis, modification abundance, rapid and highly specific target capturing features[44,45]. In this paper, an aptamer mediated MN-based biosensor will be introduced and characterized.

1.5 Thesis objectives and overview

Herein, we report a fluorescent HMN biosensor based on methacrylated hyaluronic acid (MeHA) for on-needle and reagentless capture and detection of any biomarkers of interest. HA is naturally present in the skin, and it is approved as a dermal filler by Food and Drug Administration (FDA)[46]. MeHA has been also reported as a suitable candidate for fabricating swellable HMN patches for ISF extraction and off-site target detection[24] with no toxicity[47]. Our reagentless fluorescence assay for minimally invasive detection (RFMID) integrates a rapid, and simple approach to link aptamer probes

to the MeHA matrix. We demonstrate the application of our biosensor for *ex vivo* detection of four clinically important biomolecules: glucose, whose measurement is crucial to avoiding diabetic complications; adenosine triphosphate (ATP), an important molecule that provides energy to drive many processes in living cells; L-tyrosinamide, an important amino acid which is essential to the catalytic activity of several enzymes[48] and is a biomarker of metabolic syndrome[49]; and thrombin, a proteinase that plays an imperative role in regulating hemostasis and maintaining blood coagulation systems[50]. HMN arrays functionalized with aptamer probes can detect the analyte concentrations with high sensitivity and specificity. We also show that the RFMID can be employed for tracking rising and falling levels of glucose in an animal model of diabetes. Specifically, the RFMID can accurately track severe hypoglycemia range, which cannot be detected using the commercially available glucose monitoring devices. The proposed RFMID technique is expected to pave the way for the next generation of real-time, continuous biosensors.

In the next chapter, the hydrogel that we used for RFMID fabrication, and its synthesising and characterization protocol are introduced at beginning. Next, I focus on the sensing strategy of our RFMID devices, followed with its fabrication procedure. Subsequently, we characterize the RFMID device using fourier-transform infrared spectroscopy (FTIR), scanning electron microscope (SEM) and fluorescent microscope. Moreover, other common features of HMN, such as swelling ability, mechanical strength, biocompatibility and target recovery rate are characterized.

In chapter 3, we investigate the target capture efficiency of our RMFID device under *in vitro* agarose and real porcine skin environment, respectively. Different types of analytes, protein or small molecule detection, are investigated, including glucose, ATP, L-tyrosinamide and thrombin. Besides the target capture efficiency, we also detected the target capture specificity of our RFMID device to ensure the fluorescent signal variance before and after patch application is due to the corresponding

13

target analytes. In addition, an *ex vivo* aptamer degradation experiment is conducted to ensure the aptamer can remain stable under real skin environment.

In the last chapter, we further investigate our glucose RFMID target capture efficiency using an animal model. In this *in vivo* experiment, glucose RFMID devices are used to monitor the diabetic rat blood glucose level ranging from 2.2mM to 33mM. Meanwhile, results obtained from RFMID are compared with the read-out obtained from a commercially available glucometer to evaluate the accuracy of our RFMID devices.

Chapter 2

Biomarker detection based on RFMID

This chapter brings a detailed overview of our RFMID device. In the beginning, the hydrogel polymer, MeHA and its synthesis procedure are explored. Next, the RFMID sensing strategy is introduced, followed with its fabrication and characterization experiment.

2.1 Methacrylated hyaluronic acid (MeHA)

2.1.1 Introduction to MeHA

As mentioned in chapter 1, MeHA is used for our RFMID devices fabrication, due to its great biocompatibility, rapid and sufficient ISF sampling capability, and simple synthesis manner.

HA is a type of natural glycosaminoglycan commonly found in nerve, connective, and epithelial tissues of human body[51]. It is also considered as a highly biocompatible polymer, which is safe to be widely applied in clinical, cosmetic industry, pharmacology, and drug delivery products[51]. However, the short half-life and weak mechanical strength of HA greatly narrows its implementation[52]. Therefore, the chemically modified HA (e.g., MeHA and maleimide modified HA (MAHA)) with great mechanical strength and degradation resistance but non-toxic, is desired alternatives to HA[34,52].
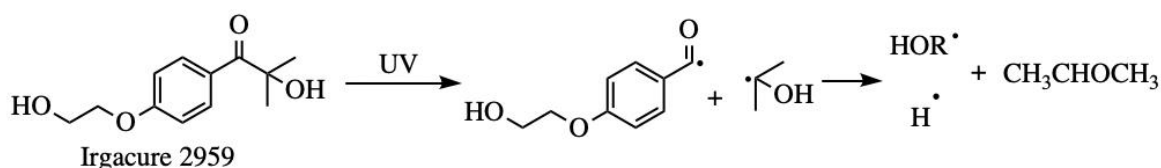
Figure 2.1 The free radical formation mechanisms of Irgacure 2959

Reported by Cheng et al., MeHA is a type of methacrylic anhydride (MA) modified HA. Under alkaline condition at 4 °C, the hydroxyl group on HA is replaced by a methacrylate group, providing a carbon-carbon double bond[24,34]. MeHA could form a covalently crosslinked polymer network with the inducing of photochemical initiator and crosslinker, along with UV treatment[24,34]. During this process,

photo initiator absorbs the UV irradiation to generate free radical (HOR·) which could attack and

activate the carbon in alkenes group[53]. Next, the activated alkenes group could link to other MeHA

Compared with the native HA, crosslinked MeHA with better rigidity and lower solubility

enhances its resistance to degradation, while its biocompatibility and moisturizing capability of MeHA

remain the same[24,34]. The internal polymer network of MeHA MN remains intact after ISF absorption,

which provides excellent swelling ability for MN patch[24]. Therefore, we choose MeHA as the

fabrication material for our RFMID devices.
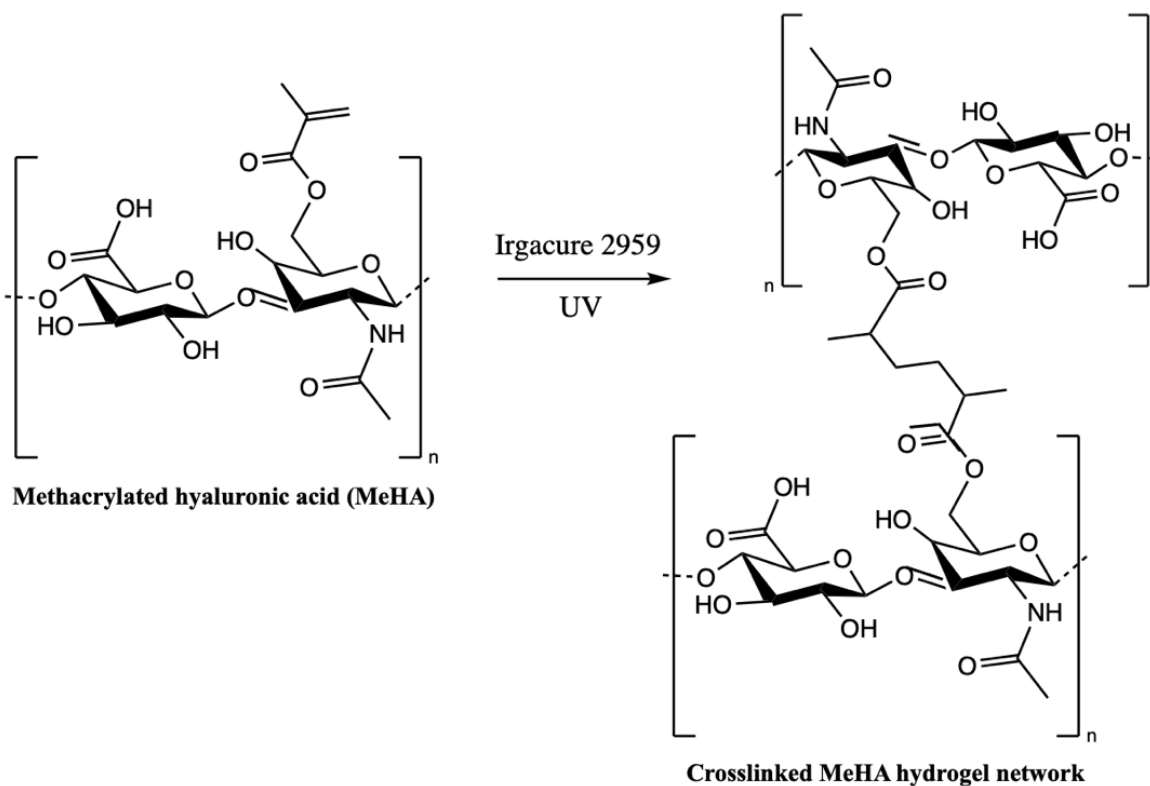
Figure 2.2 MeHA crosslink mechanism with photocleavage initiation.

16

2.1.2 Synthesis and characterization of MeHA

The MeHA was synthesized based on the modified protocol established by Poldervaart et al[34]. 2.0 g HA was dissolved in 100 mL Millipore water and stirred overnight under 4 degree for complete dissolving. Subsequently, 1.6 mL MA was added into HA solution and 3.6 mL of 5 N NaOH solution was added to adjust the solution to pH 8-9. The mixture was stirred overnight under 4 ℃ to complete the reaction. Next, MeHA was precipitated by acetone and washed three times with ethanol. Subsequently, precipitated MeHA was redissolved in Millipore water and was dialyzed for 3 days to remove the impurity. The purified MeHA was lyophilized for 3 days. Eventually, 2 -5 mg of MeHA was dissolved in 1 mL Deuterium oxide (D2O) (Sigma Aldrich, 151882) and then tested with 300MHz ^{1}HNMR with 10 ms time scale. The degree of methacrylation was determined to be 20% by integration of methacrylate proton signals at 6.1, 5.7, and 1.8 ppm to the peak at 1.9 ppm related to the N-acetyl glucosamine of HA[54] (Figure 2.3).
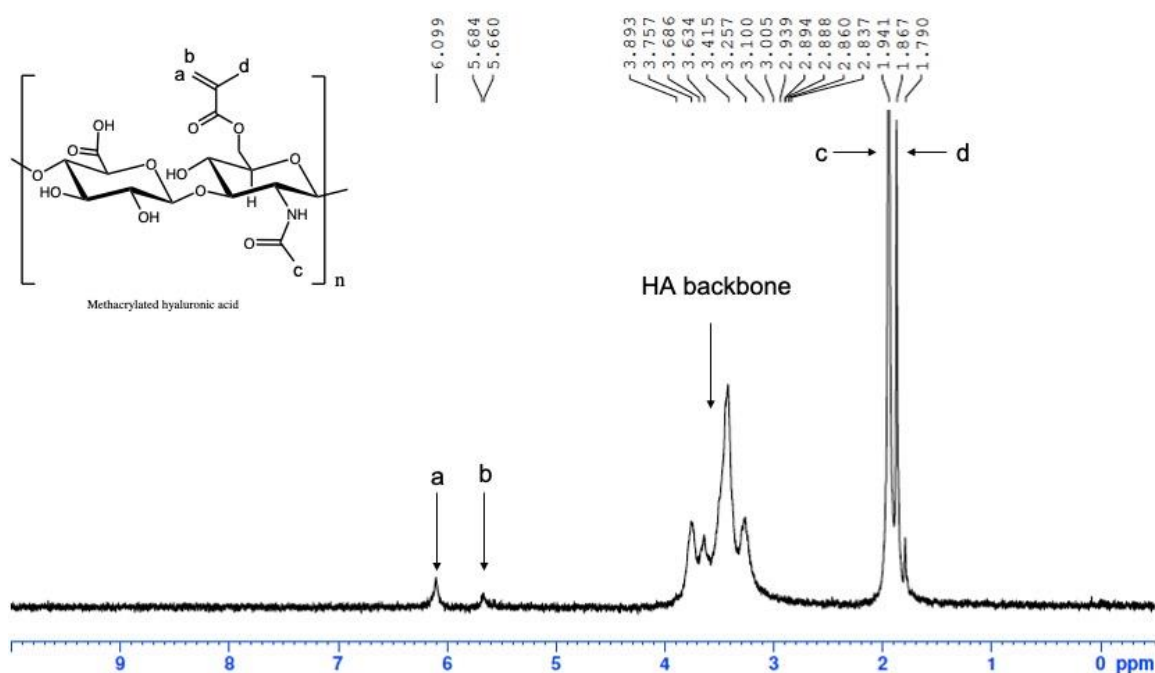
Figure 2.3 ^{1}H NMR spectra of MeHA. MeHA was characterized with 300MHz 1HNMR with 10ms time scale to determine the degree of methacrylate modification.

17

2.2 RFMID device

2.2.1 RFMID detection strategy

For reagentless target detection, we used aptamer probes and a strand displacement strategy[44,45]. Briefly, we hybridized Cy3 fluorophore-conjugated aptamers with a DNA competitor strand that has been conjugated to a quencher (Dabcyl) molecule, called the quencher strand, and coupled the complex to MeHA through covalent linkage. The aptamer-quencher complex retains the fluorophore and quencher in proximity, producing no signal in the absence of a specific target. When the aptamer binds to the target, the quencher competitor strand dissociates and alleviates quenching of the fluorophore, producing a signal without requiring for any post-processing steps such as washing or adding a detection reagent. Despite that fact that the displacement-based analyses often suffer from low sensitivities, this is not the case in our assay because the binding of an aptamer to its target molecule is more thermodynamically stable than the binding to its complementary stand[55]. Figure 2.4 shows a schematic of the RFMID reagentless detection principle.

After fabrication, the RFMID is pressed through the skin for ISF extraction and target capture. Because non-specific binding of background chemicals does not cause dissociation of the quencher strand, the probe only responds to the binding of the specific target even when the background concentration is many orders of magnitude higher. This important feature enables our sensor to operate in complex mediums such as ISF without the need for sample preparation or additional reagents.
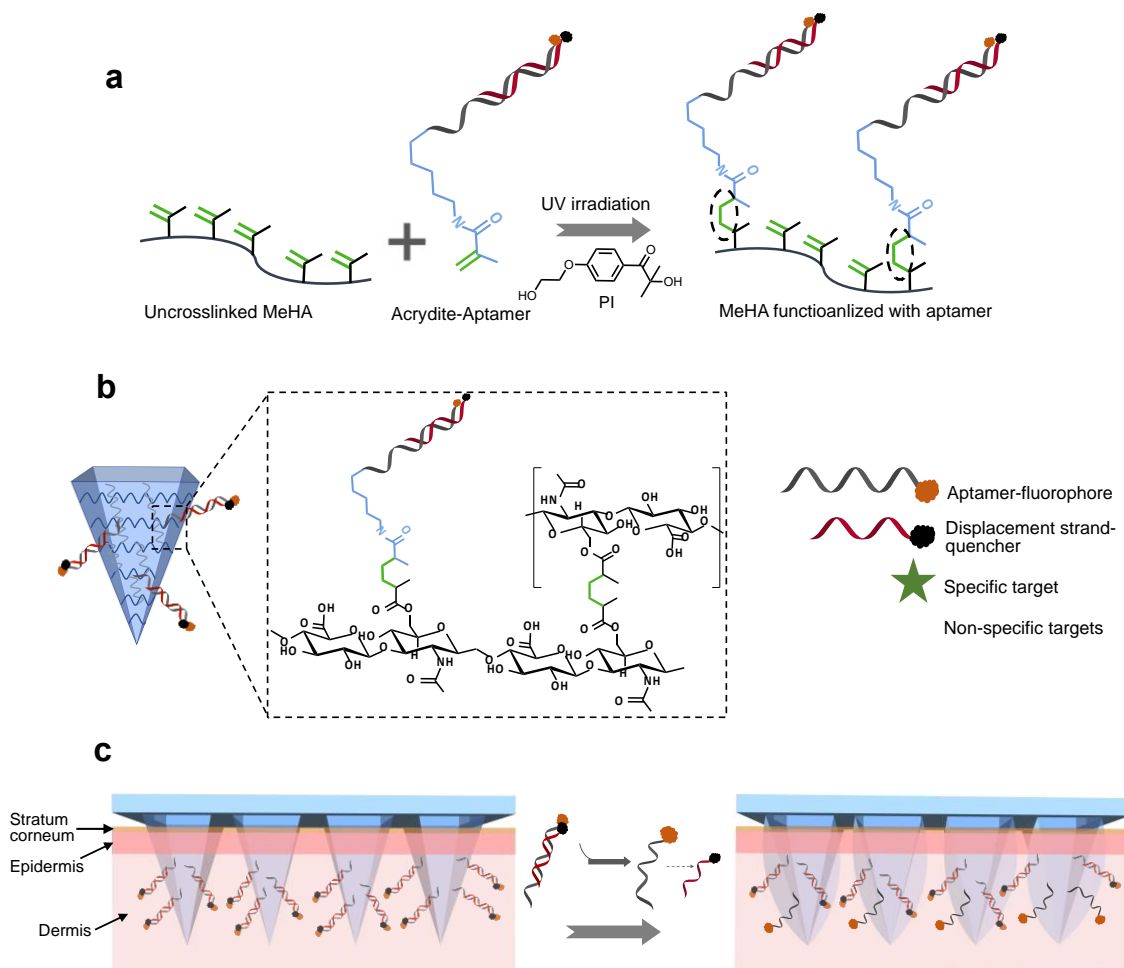
Figure 2.4 Overview of RFMID functionalization and sensing strategy. **a,** The RFMID employs a covalent binding to attach aptamer probes into MeHA. The Cy3 conjugated aptamer with an acrydite group on the 5' end is pre-hybridized with the corresponding competitor strand to form the aptamer-quencher complex, which can be covalently attached to the hydrogel matrix during the MeHA crosslinking process and in the presence of PI and under UV exposure. **b**, The RFMID's needles consist of crosslinked MeHA that is immobilized with aptamer-quencher complex. **c**, The RFMID uses a reagentless process for target detection. Upon insertion, the RFMID penetrates through stratum corneum and epidermis and rapidly swells to extract transdermal ISF. During this process, fluorophore conjugated aptamer probes selectively bind to the specific target, leading to dissociation of the quencher strand and producing fluorescent signal.

We fabricated the RFMID using a negative polydimethylsiloxane (PDMS) mold (Figure 2.5). For each RMFID patch, 50 mg MeHA, 1 mg PI and 1 mg of the crosslinking agent, N,N'-methylenebisacrylamide (MBA) were dissolved in 1.25 mL of glucose or ATP aptamer binding buffer. The MeHA solution was then sonicated for 5 min to remove the bubbles. Subsequently, 0.5mL of MeHA solution was deposited on a negative polydimethylsiloxane (PDMS) mold (Micropoint, Singapore), and degassed for 90s. After drying at room temperature for 5 hours, another 0.75 mL of MeHA solution was casted on the mold followed by drying at room temperature for 10 hrs. Next, 10 µL of aptamer-quencher strand solution composed of 1µM glucose or ATP aptamer and 10 µM corresponding quencher strand, 2 µM L-tyrosinamide aptamer and 2.5 µM quencher strand or 1uM of thrombin aptamer-quencher complex with 15 min pre-hybridization was loaded on each HMN followed by drying at 45 degrees for 30 min. Consecutive adding of MeHA solution and aptamer-quencher complex solution rather than adding a mixture of MeHA and aptamer solution at once reduces the background signal since the aptamer-quencher complex is added only to the needle area, i.e., the base of the patch does not fluoresce. Dry HMN patches were then crosslinked by UV light with 360 nm wavelength for 15 min. The RMFID patches were washed twice with 10 µM of glucose, ATP, L-tyrosinamide or thrombin aptamer binding buffer and further dried under 45 degrees. Last, MN patches were carefully separated from PDMS molds and further crosslinked for 5 mins.
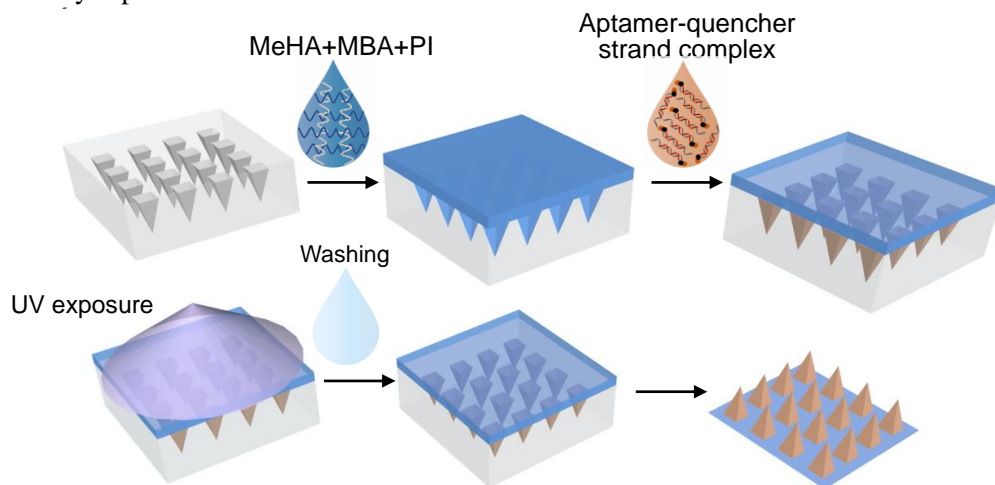
Figure 2.5 Schematic of the fabrication process of RMFID

After being trimmed and taped on a clean glass slide, the RMFID patches were observed under a Scanning electron microscopy (SEM) (Figure 2.6). The fabricated needles of the RMFID patch were 850 µm in height, 250 µm in base width and 500 in internal spacing. The needles on HMN patches are sharp that are critical for effective skin penetration[24,43].
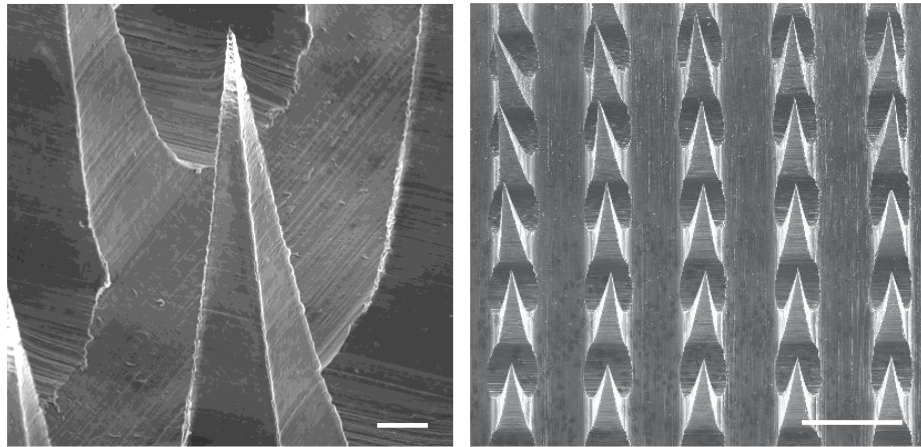
Figure 2.6 Scanning electron microscopy (SEM) images showing the morphology of fabricated RFMID from the single needle view (left) and side view (right). Scale bar, 50 µm (left) and 500 µm (right).

2.2.2 MeHA MN and RFMID device characterization

We first investigated the chemical structure of hydrogel biosensor and efficiency of linking the aptamer probes to MeHA using Fourier-transform infrared spectroscopy (FTIR, Bruker Hyperion 3000 FTIR Microscope) (Figure 2.7).
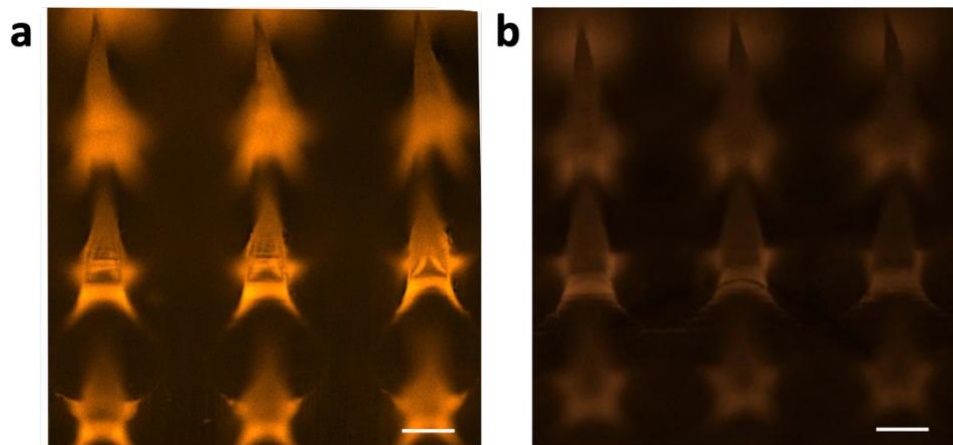
Figure 2.7 Fluorescence microscopic images of RMFID patches functionalized with **a,** aptamer probe only and **b,** aptamer-quencher complex. Scale bar, 250 µm.

The following four samples were made in 1 mL DNase-free water: two samples of 50 mg/mL MeHA solution containing 1 mg/mL photo initiator (MeHA); one sample of 50 mg/mL MeHA solution containing 1 mg/mL photo initiator and 1 mg/mL MBA (MeHA+MBA); and one sample of 50 mg/mL MeHA solution containing 1 mg/mL photo initiator and 1 µM aptamer (MeHA+APT). MeHA+MBA, MeHA+APT and one sample of MeHA were crosslinked under UV exposure for 20 min, followed with FTIR spectrum from 4000 to 400 cm^{-1}.

The spectrum of MeHA sample before UV exposure showed a strong peaks at ≈1633 cm−1 (C=C)[24], which significantly decrease in intensity after UV irradiation in MeHA sample with MBA, indicating that the carbon-carbon double bonds of MeHA were broken to form the covalent linkage with MBA. This reduction in the peak intensity was found to be minimal in the pure MeHA sample after UV irradiation. However, a similar trend with MeHA+MBA sample was observed for MeHA mixed with aptamer probes conjugated with acrydite group (MeHA+APT) after UV irradiation, suggesting a successful attachment of aptamer probes to the MeHA network.
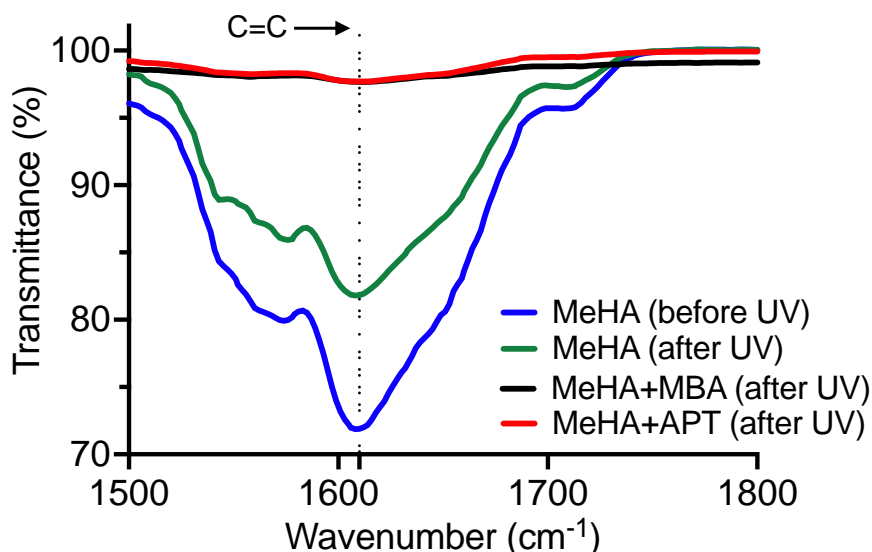
Figure 2.8 FTIR spectra of MeHA thin films before and after UV irradiation and MeHA with MBA or with ATP aptamer probe (APT) after UV irradiation. The reduction in transmittance peaks of hydrocarbyl group at 1633 cm^{-1}.

The successful aptamer linkage was also confirmed via fluorescence measurement after the fabrication process. MN patches containing aptamer-quencher complex and only aptamer probes were observed under fluorescence microscopy (NIKON, Ti2). The aptamer-only patch (Figure 2.8, i) shows an elevated fluorescence signal compared to the patch functionalized with aptamer-quencher complex (Figure 2.8, ii), demonstrating both the successful aptamer linkage and quenching capabilities of Dabcyl.
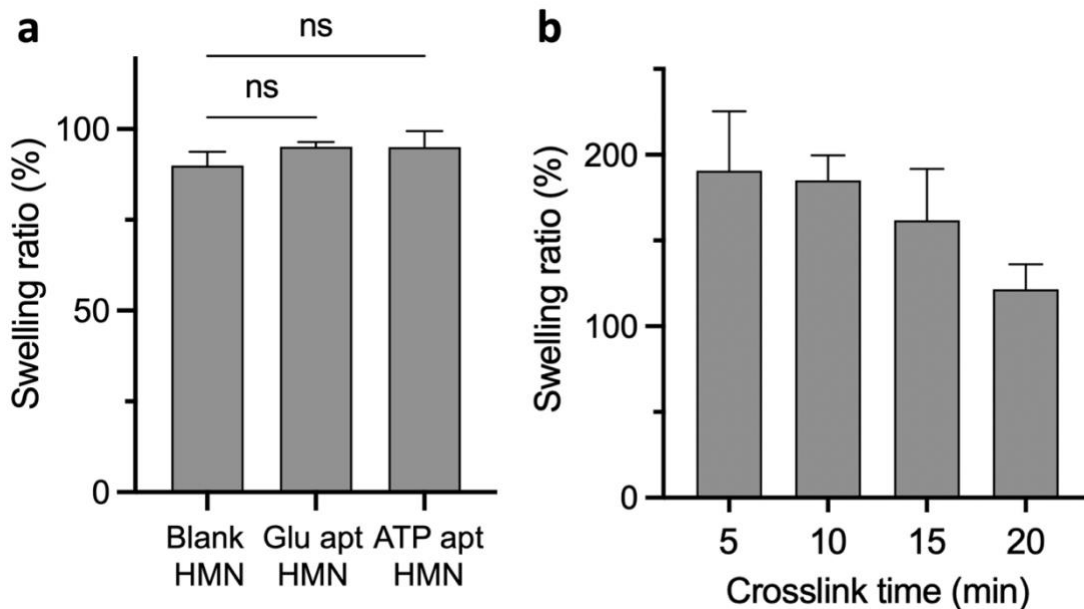
Figure 2.9 Swelling ratio of RFMID device and MeHA MN with different crosslink time. **a.** Swelling ratio of a blank HMN patch without aptamer and HMN patches functionalized with glucose or ATP aptamer probes. The presence of aptamer does not affect the swelling capability of HMN patches. The data among Glu apt HMN and ATP apt HMN groups was not significantly different from the blank HMN group (ns, not significant, $P > 0.9999$ by the ordinary one-way analysis of variance (ANOVA) with Turkey's multiple comparison test). **b,** swelling ratio of MeHA-HMNs with various crosslinking time (5, 10, 15, 20 min). all the data are present in the form of mean $\pm$ s.d. n = 3 repeated tests per group.

We next investigated the effect of aptamer probes on the swelling capability and mechanical strength of the RFMID patches. The dry mass (W_0) of blank and aptamer probe functionalized HMNs were measured. Then the HMNs were penetrated to a 1.4wt % agarose (Sigma Aldrich, A0169) through a layer of parafilm and swelled for 10 min. The wet mass (W_t) of the swelled HMN patches was measured afterwards. The swelling ratio of HMNs was calculated based on the below formula:

$$swelling\ ratio\ = \frac{W_t - W_0}{W_0} \times 100\%$$

We observed that the presence of aptamer probes does not have any significant effect on the swelling ability of MeHA hydrogel network (Figure 2.9a). The slight increase in the swelling might be due to the lower crosslinking density in the RFMID patches (Figure 2.4b). We also observed a reduction of swelling by extending the crosslinking period (Figure 2.9b), which agrees with previous work reported on MeHA-HMNs[24]. In this experiment, the swelling ratio was measured and calculated following the procedure shown above, but the HMN patches without aptamer probe immobilization are crosslinked with different time length.
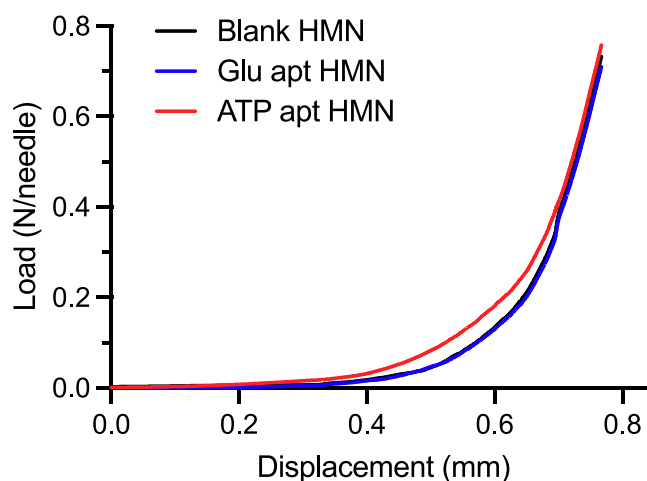
Figure 2.10 Mechanical compression test for blank HMN and HMN patches functionalized with glucose and ATP aptamer probe.

The mechanical strength of MeHA-HMN patch was also evaluated through a compression test. The mechanical strength of MN patches was measured using Instron 5548 micro tester equipped with 500N compression loading cell. For each test, the HMN patch was placed flat on its backside (tips facing upwards) on a compression platen. The distance between two platens was set to 1.5 mm. A vertical force was applied (at a constant speed of 0.5 mm/min) by the other platen. The compression loading cell capacity was set to 70 N. The load (force; N) and displacement (distance; mm) was recorded by the testing machine every 0.1 s to create the load-displacement curve. HMN patches with

and without aptamer show similar load versus displacement profiles (Figure 2.10), which indicates the mechanical strength is not influenced by the aptamer probes. The compression test result also shows that HMNs in this study can exert more than 0.6 N, which is sufficient for successful piercing through the skin[24].

The capability of the RFMID for target capture or recovery was investigated using glucose as a target molecule via testing three HMN samples; a blank HMN patch with no aptamer probes, a HMN patch functionalized with glucose aptamer probes (Glu apt HMN), and a HMN patch functionalized with glucose aptamer probes where upon target capture the aptamer probes were degraded using ultrasonication (Glu apt-US HMN)[56] (Figure 2.11a). After measuring the dry mass (W_0), HMNs were penetrated to 1.4 wt% agarose containing varying glucose concentration of 3.5, 5, 10, 20 mM for 10 min. After measuring the wet mass (W_t), Glu apt-US HMN was sonicated for 10 min and named as. Subsequently, all the HMN were mixed with 300 μL (V) Millipore water in a centrifuge tube followed by 5 min centrifugation at 2,100 rcf. Subsequently, 250 μL of recovered solution was transferred into a 96-well plate for the recovered glucose concentration measuremnt using a glucose (GO) assay kit (Sigma, GAGO20). Glucose recovery rate was defined by the following formula:

$$Glucose\ recovery\ rate = \frac{C_t \times V}{C_0 \times (W_t \times W_0) \div \rho} \times 100\%$$

C_0 refers to the initial glucose concentrations (3.5, 5, 10, 20 mM), C_t is the detected glucose concentration recovered from MN, V is the volume of recovered solution (300 μL), $(W_t - W_0) \div \rho$ is the volume of solution absorbed by HMN.

The purpose of this experiment is to study the importance of the presence of aptamer probes for retaining the target analytes. The three HMN patches were then pressed through an agarose hydrogel loaded with varying concentrations of glucose. The diffused or captured targets by blank HMN and Glu apt HMN were then recovered by centrifugation. For Glu apt-US HMN, prior to centrifugation, the

patches were sonicated that results in the aptamer degradation, thus releasing the captured targets into the recovery solution.
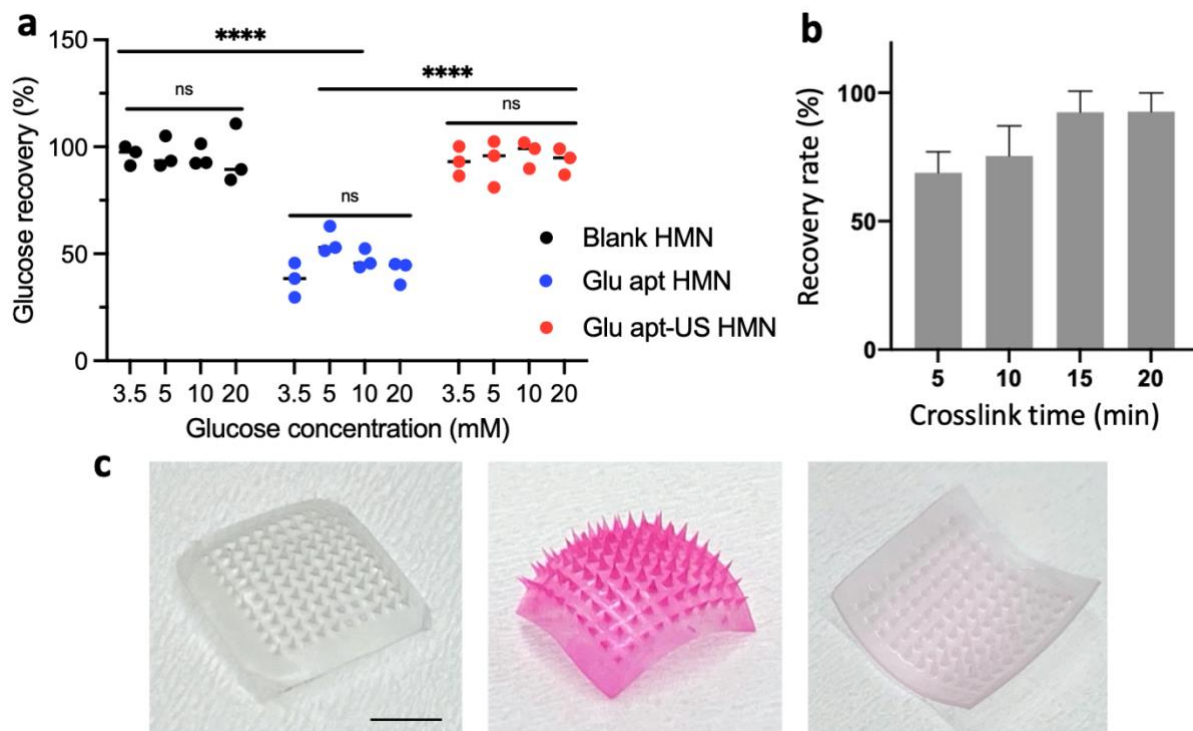
Figure 2.11 Target recovery characterization of RFMID and MeHA MN with different corsslink time. **a**, A blank HMN patch and HMN patches functionalized with the glucose aptamer probes (Glu apt HMN) were inserted into agarose hydrogels containing various concentrations of glucose (3.5, 5, 10, 20 mM) for 10 min to capture or recover glucose. For one group of aptamer HMNs, upon target capture, the aptamer probes were degraded by sonication (Glu apt-US HMN). Glucose was then recovered by centrifugation. Data in Blank HMN and Glu apt-US HMN groups are significantly higher than Glu apt HMN group (****$P < 0.0001$ by two-way ANOVA with Geisser-Greenhouse correction). Among each group, data of various glucose concentration group is not significantly different (ns, not significant, $P > 0.9999$ by two-way ANOVA with Geisser-Greenhouse correction). **b**, Rhodamine B recovery rate of MeHA-HMNs with various crosslinking time (5, 10, 15, 20 min). **c**, Optical images of a HMN patch before (left) after (middle) solution extraction from an agarose hydrogel containing 100 mg/mL RhoB, followed by the RhoB recovery (right). Scale bar, 5 mm. Data is expressed as mean ± s.d. n = 3 replications per group.

As shown in Figure 2.11a, the blank HMN and Glu apt-US HMN show a high recovery rate where the absence and the degradation of aptamer probes, respectively, allow for the release and recovery of the target molecules. While in Glu apt HMN sample, the presence of aptamer probes hinders the full recovery of glucose. This experiment indicates that the analytes diffuse into the patch needles and are captured by aptamer probes for subsequent detection and confirms that the presence of an intact,

26

functional aptamer is required for target capture. To visualize the target recovery capability, HMN patches were pressed through an agarose hydrogel loaded with Rhodamine B (RhoB) then the diffused dye was recovered (Figure 2.11 b&c).

Chapter 3

In vitro and *ex vivo* characterization

3.1 *In vitro* target capture efficiency detection of RFMID

3.1.1 Aptamer probe target capturing characterization

To investigate our sensor's capability for biomolecule detection, we first studied the capability of the aptamer-quencher strand complex for target detection and optimized the ratio of aptamer to quencher strand (Figure 3.1). The aptamer probe was hybridized to its corresponding quencher for 30 min before adding the targets. Subsequently, the fluorescence intensity difference was tracked with plate reader for 30 min.
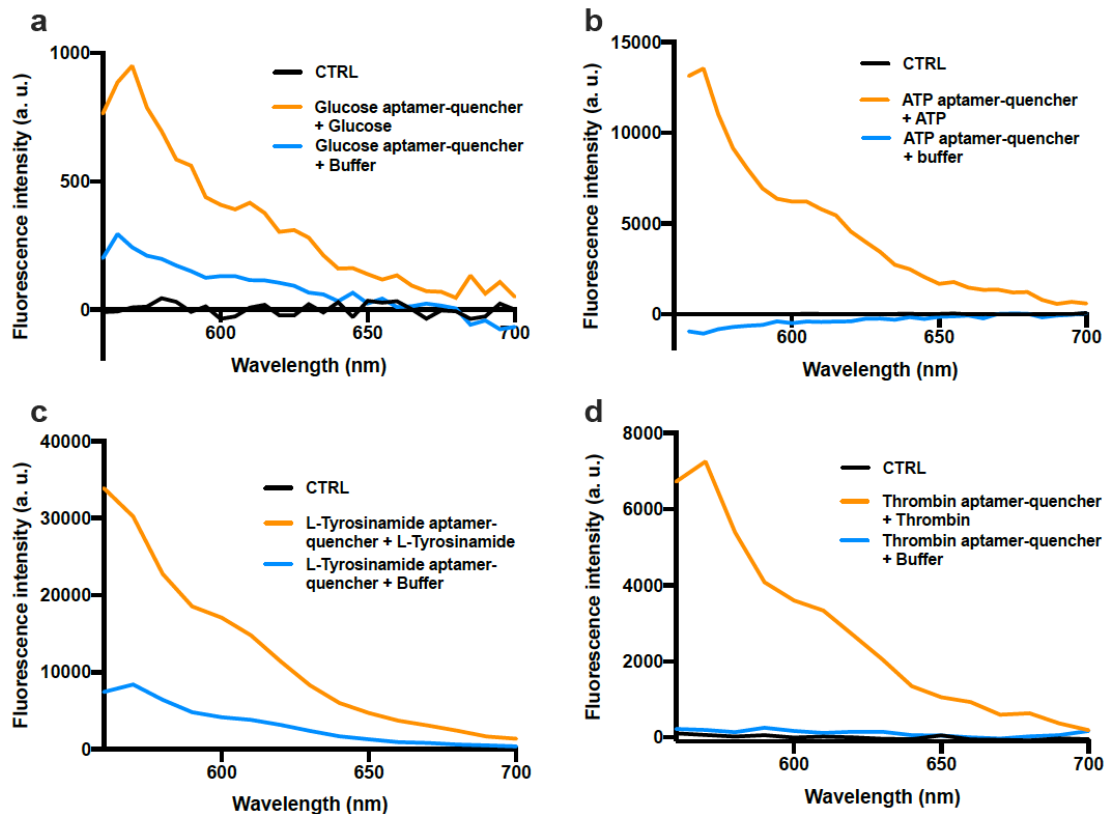
Figure 3.1 Assessment of aptamer binding efficiency. The target binding efficiency of **a,** glucose, **b,** ATP, **c,** L-Tyrosinamide, and **d,** thrombin aptamer was tested with spectrophotometer.

3.1.2 Glucose, ATP, L-tyrosinamide and thrombin RFMID target capture efficiency characterization using agarose hydrogel

Next, a series of experiments were conducted to measure varying concentrations of glucose (Figure 3.2a), ATP (Figure 3.2b), L-tyrosinamide (Figure 3.2c), and thrombin (Figure 3.2d) *in vitro* using HMNs linked with aptamer-quencher strand complex. For glucose[57,58], ATP[59], and L-tyrosinamide measurement[60], the specific aptamer probes were hybridized to a quencher strand while for thrombin measurement, the aptamer probe was linked to the quencher strand via a polyethylene glycol (PEG) linker[44], averting the release of the quencher strand upon target binding.
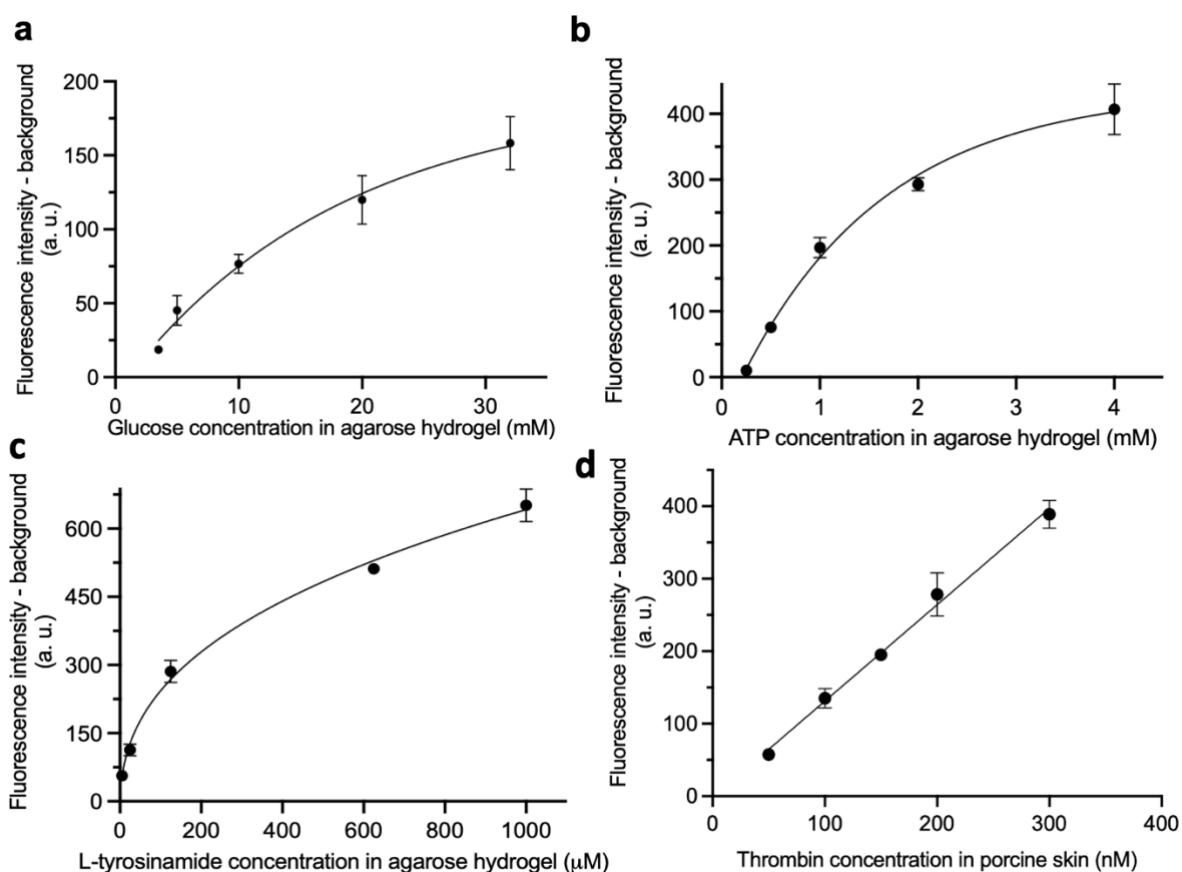
Figure 3.2 *In vitro* characterization of RFMID using an agarose hydrogel model. The RFMID devices functionalized with **a**, glucose **b**, ATP **c**, L-tyrosinamide or **d**, thrombin aptamer-quencher complex was applied into agarose hydrogels containing varying concentrations of glucose (3.5, 5, 10, 20, 32 mM), ATP (0.25, 0.5, 1, 2, 4 mM), L-tyrosinamide (5, 25, 125, 625, 1000 µM), or thrombin (50, 100, 150, 200, 300 nM) for 10 min. Each experiment was repeated three times. Data are presented as mean ± s.d. a.u., arbitrary units.

In this experiment, the Fluorescence intensity (FI) of RFMID was recorded by the fluorescent microscope from the base side with 10 ms exposure time. The RFMID patches were applied on 1.4 wt% agarose hydrogels containing various concentrations of ATP (0, 0.25, 0.5, 1, 2, 4 mM), glucose (0, 3.5, 5, 10, 20, 32 mM), L-tyrosinamide (0, 5, 25, 125, 625, 1000 µM) or thrombin (0, 50, 100, 150, 200, 300 nM) for 10 min, respectively. Next, the fluorescent intensity of the RFMID after target detection was recorded. Finally, the corresponding needles were identified and the fluorescence intensity difference before and after target capturing were measured and calculated by subtracting FI before target capture from the FI after target capture.

We observed that by increasing the target concentration, the signal intensity increases, demonstrating the target capture and dissociation of the quencher strand. Figure 3.3 show that the fluorescence intensity of MN patches increases with the rising glucose and ATP concentration, respectively, confirming elevated dissociation of quencher strand and target capture.
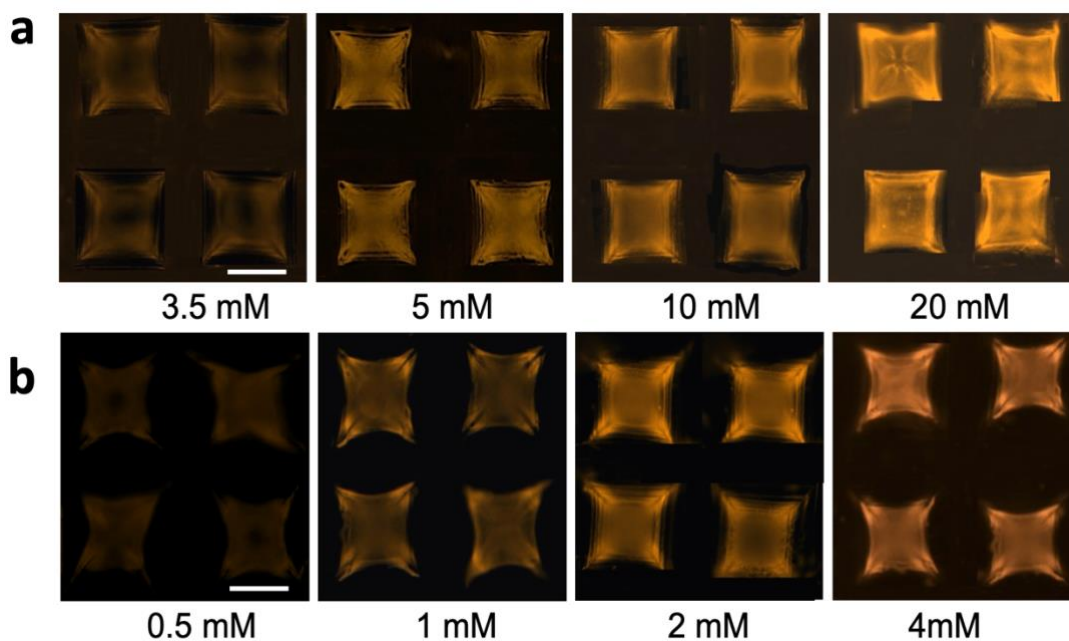
Figure 3.3 Fluorescence microscopic images of **a,** glucose-RFMID and **b,** ATP-RFMID after capturing varying concentrations of ATP (0.5, 1, 2, 4 mM) or glucose (3.5, 5, 10, 20, 32 mM) in the agarose hydrogel.

3.1.3 Cross-reactivity and stability characterization of RFMID device

To further explore the sensitivity and reliability of detection, cross-reactivity among glucose and ATP was examined by applying HMN patches functionalized with glucose (ATP) aptamer into an agarose hydrogel loaded with a definite concentration of glucose (ATP) while the concentrations of ATP (glucose) increased. We observed that for both glucose and ATP, the changes of the fluorescence intensity for the non-specific target were almost unnoticeable, indicating the high selectivity of the sensor (Figure 3.4a). The cross-reactivity of RFMID device for glucose detection was also studied against fructose, uric acid, insulin, 3-β-Hydroxybutyrate- the dominant biomarker of ketone formation[61] (Figure 3.4b). We observed that the addition of common interfering agents (with a concentration higher than their physiological levels) does not affect the RFMID measurement which confirms excellent selectivity of the sensor.
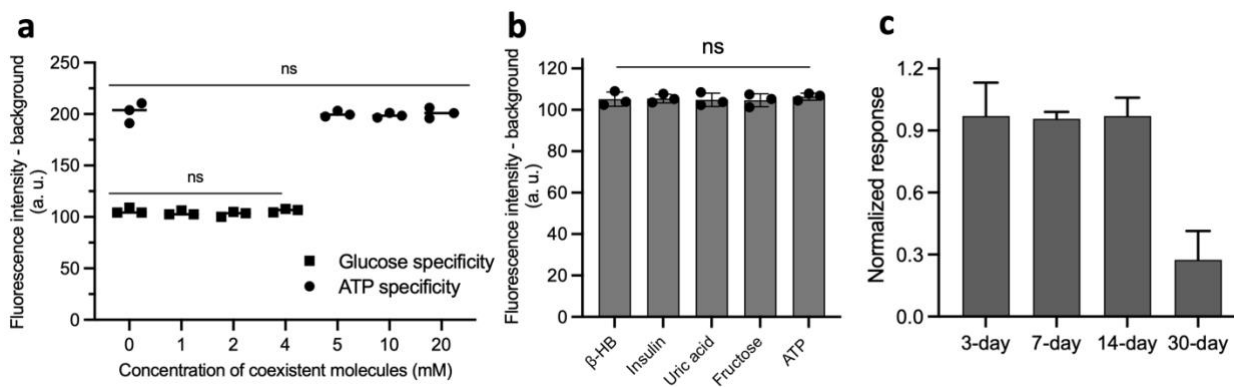
Figure 3.4 *In vitro* characterization of RFMID devices. **a,** specificity of RFMID devices for specific target capturing was tested. The ATP-RFMID devices were applied into agarose hydrogels containing 1 mM of ATP while glucose concentrations increased (0, 5, 10, 20 mM). Similarly, the glucose-RFMID devices were applied into agarose hydrogel containing 20 mM of glucose while ATP concentrations increased (0, 1, 2, 4 mM). **b,** cross-reactivity of RFMID device for glucose capture in the presence of common interfering agents was studied. In this experiment, agarose hydrogel was loaded with a 20mM glucose, 10mM β-HB, 10nM insulin, 0.5mM fructose, 0.5mM uric acid or 4mM ATP. **c,** stability test of RFMID patch for glucose measurement. Glucose-RFMID patches were stored at the room temperature for 3, 7, 14 or 30 days and then were applied to agarose hydrogel loaded with 20 mM glucose. The responses were normalized to the measurements extracted from a fresh RFMID patch. Data is expressed as mean $\pm$ s.d. n $=$ 3 replications per group (ns, not significant).

We have also studied the storage stability of glucose-RFMID patches. A group of glucose-RFMID patches were prepared following the protocol mentioned in RFMID fabrication section. The freshly prepared glucose-RFMID patches were applied on an agarose hydrogel containing 20 mM glucose to determine the target capture efficiency. The result was used as positive control (Day 0). The rest of glucose-RFMID patches were stored in a photophobic nitrogen desiccator at room temperature for 3, 7, 14 and 30 days followed with glucose capture efficiency detection. The glucose capture efficiency for these groups was normalized to the control group and compared. The results have shown that the patches can be stored for 14 days at the room temperature with negligible effect on signal measurement (Figure 3.4c).

3.2 *Ex vivo* targets capture efficiency detection of RFMID

3.2.1 RFMID stability characterization under real skin environment

Upon successful detection of target analytes in agarose hydrogel, the sensor capability for in situ biomarker measurement was tested using an *ex vivo* skin model. Glucose RFMID patches were applied to the porcine ear skin for 5 min with index finger pressure. After removing the RFMID patches, skin samples were imaged with digital camera for 13 min with a 5 min interval to observe the micro-sized holes left by RFMID. Microneedle traces were evident in the porcine skin, showing an efficient skin penetration (Figure 3.5).
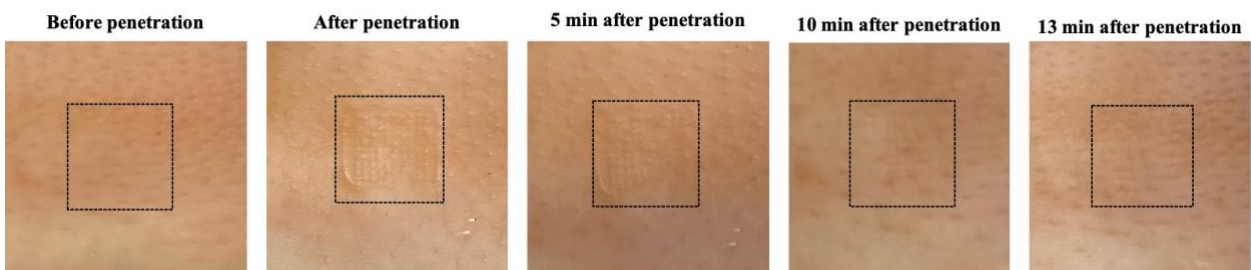
Figure 3.5 *Ex vivo* porcine skin penetration efficiency test using RFMID.

Subsequently, the stability of aptamer probes in the skin environment against nucleases present in the skin was examined. To this end, a serious of MeHA-HMNs linked with 1 µM glucose, ATP, L-tyrosinamide, or thrombin aptamer probes only were prepared. After washing and crosslinking, the fluorescent intensity of these HMN patches were measured and recorded, followed with blank agarose hydrogel or pre-equilibrated porcine skin penetration for 10 min or 5 min, respectively. Next, 10 µL of corresponding quencher solution was applied on top of the HMN, followed with 40 min air-drying. The concentrations of aptamer and quencher solution casted on the HMN patches are the same as the RFMID fabrication section. The fluorescent intensity difference before and after aptamer-quencher hybridization was calculated and compared between the agarose and porcine skin insertion, and the percentage of the aptamer probes that remained stable against nuclease present in the skin was calculated.
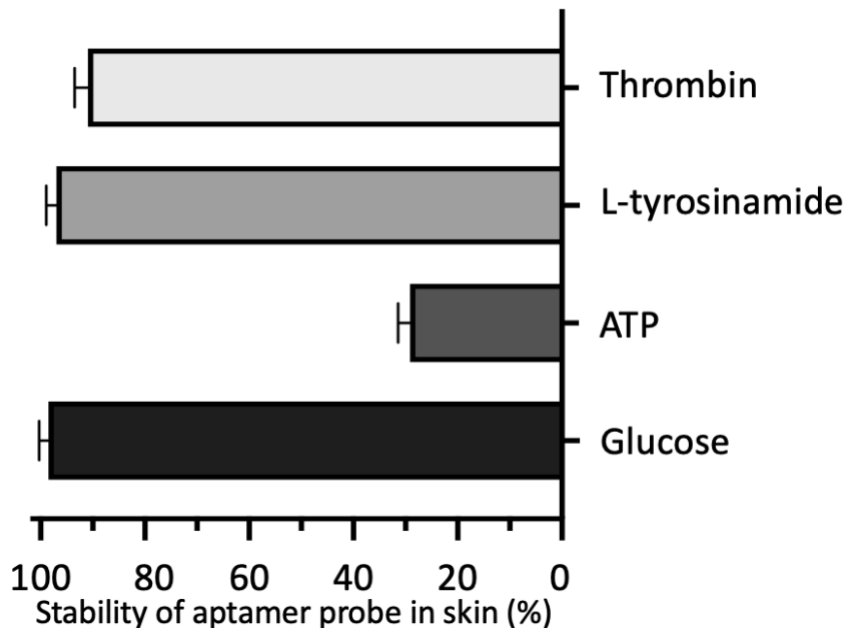
Figure 3.6 Stability of the aptamer probes in the skin. RFMID patches functionalized with only aptamer probes were applied to porcine skin or a blank agarose hydrogel. The reduction of fluorescence signal intensity of the patches applied to skin or agarose were then measured and compared. The graph shows 1-[(fa-fs)/fa] as a measure of aptamer stability, where fa and fs are the reduction in fluorescence signal for HMN patches applied into the agarose hydrogel or skin, respectively, upon addition of quencher strands.

We observed that the fluorescence intensity of the patches did not change after insertion. After penetration, the quencher strand was added to the HMN patches and a reduction in fluorescence signal was observed. The reduction of fluorescence signal intensity of the patches applied to skin or agarose were then measured and compared. The fluorescence signal reduction in HMNs penetrated through skin was 98%, 29%, 97%, and 91% of the ones inserted into blank agarose hydrogel for glucose, ATP, L-tyrosinamide, and thrombin aptamer probes, respectively, (Figure 3.6) indicating that most of ATP aptamers became degraded in the skin and could not be hybridized to the corresponded quencher strands. These results confirm that the glucose, L-tyrosinamide, and thrombin aptamers have a great stability in skin while the ATP aptamer might not be sufficiently stable to permit target detection in a complex ISF environment.

3.2.2 Glucose, ATP, L-tyrosinamide and thrombin RFMID target capture efficiency detection using porcine ear skin

The RFMID was then employed for glucose (Figure 3.7a), ATP (Figure 3.7b), L-tyrosinamide (Figure 3.7c), and thrombin (Figure 3.7d) detection using porcine skin equilibrated with different concentrations of the target analytes. To this end, porcine ear skin were rinsed with DI water and trimmed to 1 cm by 1 cm square, then equilibrated in 1×PBS with various concentrations of ATP (0, 0.25, 0.5, 1, 2, 4 mM) or glucose (0, 3.5, 5, 10, 20, 32 mM), L-tyrosinamide (0, 5, 25, 125, 625, 1000 µM) or thrombin (0, 50, 100, 150, 200, 300 nM) overnight. Subsequently, ATP, glucose, L-tyrosinamide, or thrombin RFMID patches were applied on the target porcine skin for 5 min, respectively. Tegaderm tape (3M) was used to fix RFMID patches on the skin. The fluorescence signal intensity was measured before and after applying the patches and the difference in signal intensity was reported. Similar to the *in vitro* experiment, the fluorescent intensity difference of RFMID before and after target capturing was calculated. We used these data to construct standard curves that correlate fluorescence signal intensity to target concentration in skin ISF. We estimated the limit of detection (LOD) of our biosensor to be three times the standard deviation of the fluorescence signal intensity

from a blank agarose hydrogel. Our device achieved a LOD of 1.1 mM for glucose, 0.1 mM for ATP, 3.5 μM for L-tyrosinamide and 25 nM for thrombin measurements in skin ISF. Our glucose detection limit and dynamic range cover the clinical hypoglycemia, euglycemia and hyperglycemic ranges. Our system can potentially be employed to reliably quantify pre- and post-prandial glucose concentrations in patients with diabetes while the accuracy of most of commercially available glucose monitoring devices is still the lowest within the hypoglycemic range[62].
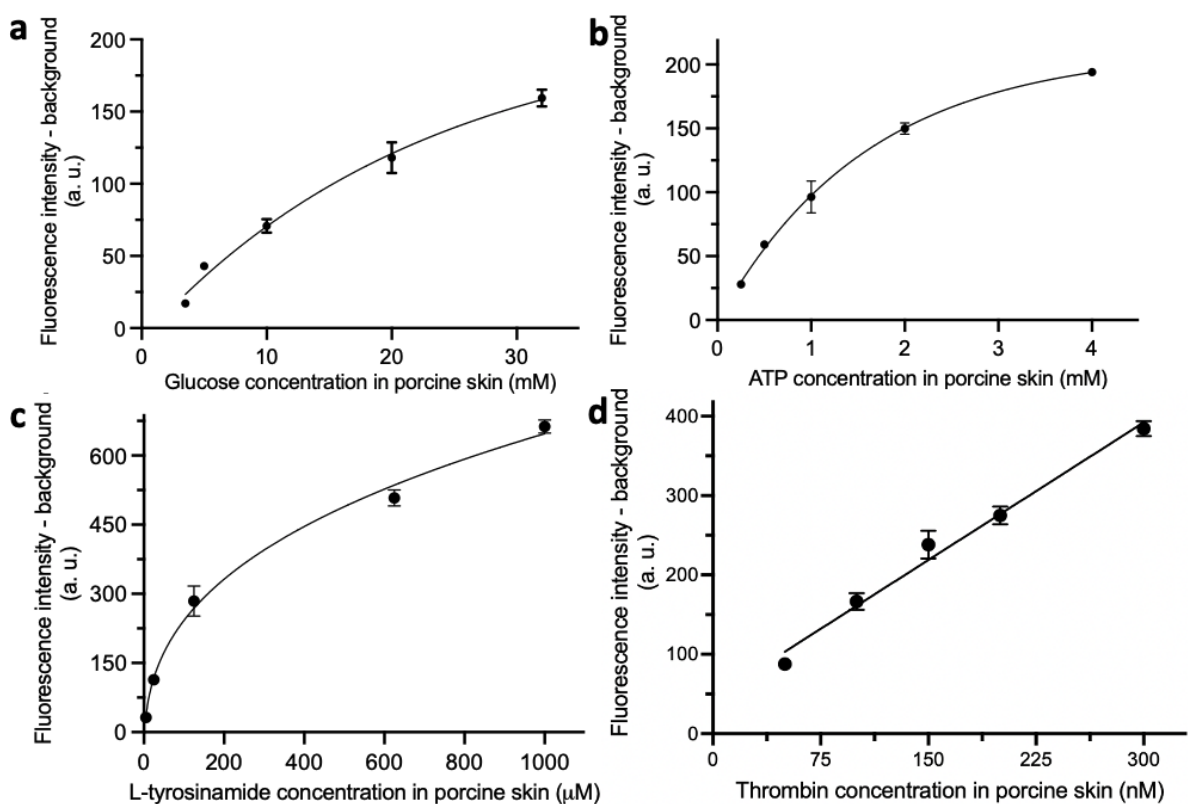
Figure 3.7 The RFMID devices functionalized with a, glucose b, ATP c, L-tyrosinamide or e, thrombin aptamer-quencher complex was applied into porcine skin equilibrated with varying concentration of target analytes for 5 min. Since some ATP aptamer probes are degraded in skin (based on experiments in 3.5), the level of fluorescence signal is less compared with agarose hydrogel experiment in Figure 3.2b. Data is expressed as mean ± s.d. a.u., arbitrary units, n = 3 replications per group.

To determine the shortest timescale for effective capture of target analytes, glucose-RFMID patches were applied on the porcine skin equilibrated with various concentrations of glucose for different durations. 2 min of microneedle patch administration was found to be sufficient to capture and

detect glucose (Figure 3.8) and longer administration (5 and 10 min) did not change the measured fluorescence. The fast response is because of the swelling characteristic of MeHA-HMNs that can reach their maximum swelling within 2 min, enabling increased and rapid ISF extraction and thus target capture. The 2 min response time is also independent of the target concentration and increased glucose concentration does not affect the time needed for the target molecules to diffuse into the patch needles. Previously reported MN-based diagnostic devices require at least 140 min to detect the target analytes (Table 3.1), including the time needed for MN application, washing, and adding the detection agents[25,33,43].
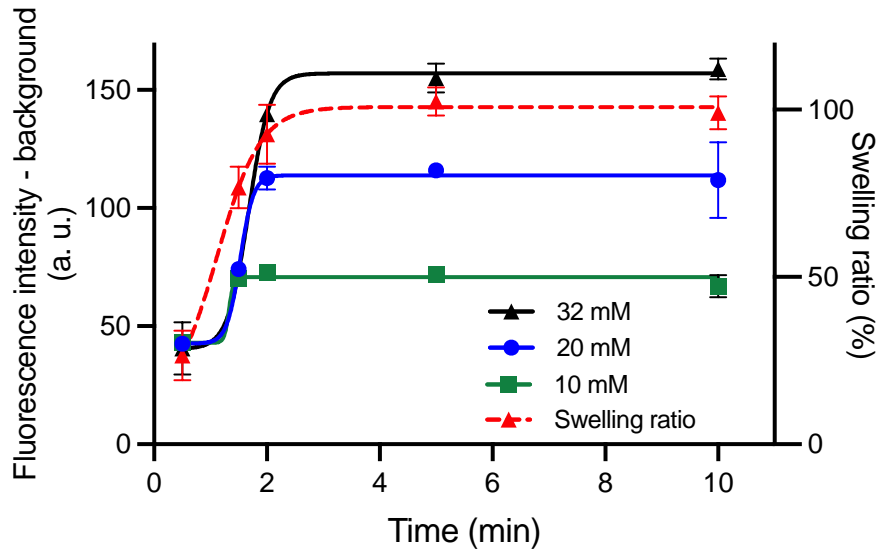
Figure 3.8 Glucose-RFMID devices were applied through porcine skin equilibrated with different glucose concentrations (10, 20, and 32 mM) for different durations. The swelling of patches and the fluorescence response were then measured. Data are presented as mean ± s.d. a.u., arbitrary units.

Table 3.1 Comparison of RFMID's response time with similar MN-based sensors

	Capture	Washing	Blocking	Detection	Washing	Total time
FLISA[43]	30 s-20 min	10 min	30 min	120 min incubation with Ab + 30 min incubation with plasmonic fluor	10 min	200 min-220 min
Aptamer decorated MN array[33]	60 min	10 min	-	60 min incubation with FAM labeled aptamer	10 min	140 min
Encoded MNs[25]	40 min	10 min	-	120 min incubation with detection Ab	10 min	180 min
RFMID	2 min	-	-	-	-	2 min

36

The change in the volume of needles after insertion was also tracked under microscope (Figure 3.9). We observed that the volume of the needles increases and reaches to a maximum upon a 2 min insertion, confirming that a 2 min insertion is needed to reach the maximum swelling. The results of *in vitro* and *ex vivo* characterizations corroborate that our system can be applied for rapid measurement of a diverse range of biomarkers, proteins, or small molecules, introducing a generalizable platform for biomolecule quantification.
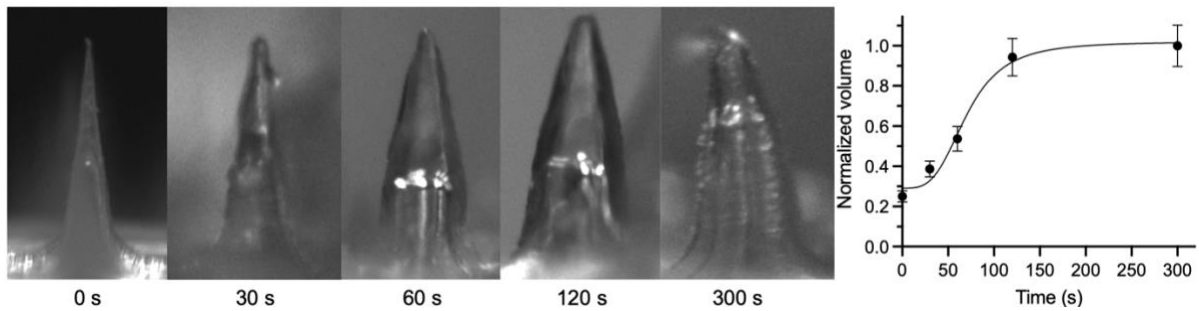
Figure 3.9 HMN patches were applied on agarose hydrogel for different durations (0, 30 s, 60 s, 90 s, 120 s, and 300 s) and the changed in the needle volume was observed on the microscope. Data is expressed as mean $\pm$ s.d. n $=$ 3 replications per group.

Chapter 4

In vivo glucose detection in animal models of diabetes

4.1 Biocompatibility evaluation of RFMID devices

Having demonstrated our platform's ability to detect glucose *in vitro* and *ex vivo* sensitively and accurately, we evaluated its performance *in vivo* using a streptozotocin-induced rat model of diabetes. Prior to the animal experiment, the cytotoxicity of the composite materials was evaluated in NIH-3T3 fibroblast cells using MTT assay (Figure 4.1). In this experiment, cells were seeded at a density of 50,000 cells per well in a 96-well plate with a final volume of 100 µL. Subsequently, cells were exposed to 10 µL of sample solution containing 10 mg/mL MeHA, 0.2mg/mL MBA, 0.2mg/mL photo initiator and 0.2 µM ATP or glucose aptamer solution. DMEM cell culture media was used as control. After 24 h sample exposure, 10 µL of the 5 mg/ml Methylthiazolyldiphenyl-tetrazolium bromide (MTT) (Sigma Aldrich, M5655) solution was added to all wells, followed with 3h incubation protected from the light. Next, 150 µL DMSO was added and gently pipetted to release the formazan crystals. The absorbance of the samples was then obtained at 540 nm using a spectrophotometer. Results showed that NIH-3T3 fibroblast viability was not significantly influenced, suggesting that the RFMID materials were biocompatible.
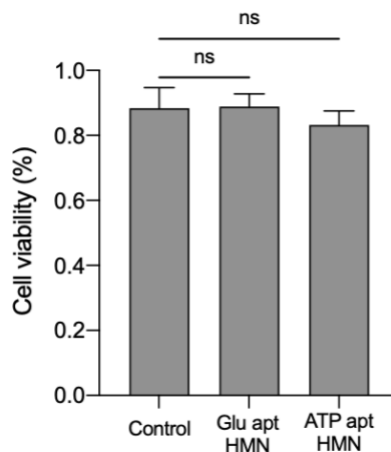
Figure 4.1 *In vitro* biocompatibility test of aptamer MeHA HMN. Mouse fibroblast cells were cultured at 100,000 cells per well in a 96-well plate and exposed to 10 µL of MeHA samples solution for 24 hours. Data is expressed as mean ± s.d. n = 3 replications per group

We have also examined the local inflammatory response against HMN patches through performing haematoxylin and eosin (H&E) staining for the evidence of inflammation in the penetration sites and surrounding subcutaneous tissue[63,64] (Figure 4.2a). Blank MeHA-HMN and glucose-RFMID patches were applied on the shaved back skin of a rat for 1 hr. The rat was euthanized after removing the MN patches, and the back skin with the dermal micropores location in the center was cut and washed with 0.9% NaCl solution. The sample was fixed with neutral buffered 10% formalin for 24 hr, then stored in 70% ethanol at -20 degrees. The embedding, section and H&E staining were conducted by PhotoMedicine Labs (PML) in the Department of Systems Design Engineering at the University of Waterloo. Histopathology image scanning was performed by Huron Technologies International Inc., Canada. There was no visible difference in histological appearance between the control skin with no patch application, glucose-RFMID patch, or blank MeHA patch. The swollen needles also remained intact following *in vivo* application (Figure 4.2b).
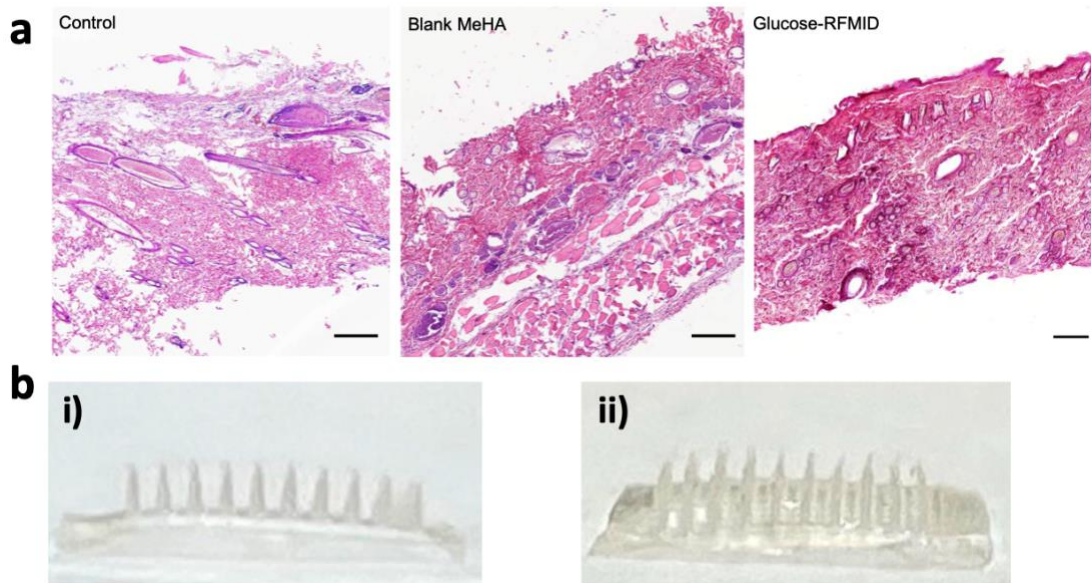
Figure 4.2 *In vivo* biocompatibility experiment **a,** Hematoxylin and eosin (H&E) staining results to study the inflammation response. Glucose-RFMID patch (right) or blank MeHA patch (middle) was applied on the rat skin for 1 hr. The treated parts of the skin were collected post MN removal. No skin inflammation at the MN-treated was observed compared to the control skin with no patch application (left). Scale bar is 400 µm. **b,** Images of HMN patch **i)** before and **ii)** after insertion into the rat skin, indicating that, despite extensive swelling, the microneedles are intact after removal from the skin.

4.2 Glucose RFMID characterization in diabetic rats

RFMID patches were inserted on the rat's dorsal skin (Figure 4.3a). HMN patches efficiently penetrated the tissue as evidenced by the microneedle traces and the skin recovered well post-treatment (Figure 4.3b). The HMN punctures disappeared gradually within 15 min of removing the patch. This is due to the biocompatibility and minimal invasiveness of the RFMID patches. The diabetic rats were fasted for 5 hours prior to the experiment and treated first with 4 IU kg^{-1} dose of human recombinant insulin subcutaneously to lower blood glucose and after hypoglycemia was reached with 30% glucose intraperitoneally to increase blood glucose again.
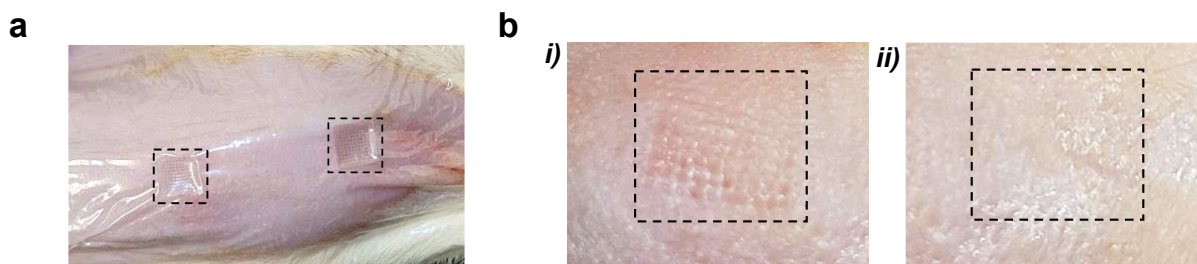
Figure 4.3 a, RFMID patches were applied into the dorsal skin of awake rats and fixed with Tegaderm tapes for 5 min. **b,** Magnified images of the trace of a patch **i)** on the skin and **ii)** 15 min after removing the patch

All the animal studies were performed in accordance with the Guidelines for the Care and Use of Laboratory Animals and the Animal Welfare Act Regulations; all protocols were approved by the University of Toronto Institutional Animal Care and Use Committee. An established model of T1D, the streptozotocin (STZ)-induced diabetic rat, was used to explore the *in vivo* performance of RFMID. Male Sprague Dawley rats (Charles River, 100-150 gr) were injected with STZ (65 mg/kg i.p.) that destroys the host's pancreatic beta-cells secreting insulin[44]. After the STZ injection, the rats were monitored for 1 week and their blood glucose was measured every 2 days using a glucose meter (OneTouch® Ultra®, LifeScan, Inc., USA). Diabetic rats with blood sugar stabilized above 17 mM were selected for this study. Before starting experiments, the rats were fasted for 5 hours. Rat skin was then shaven, treated with hair removal cream, and dried prior to MN patch application. RFMID patches for ISF glucose detection were prepared and their fluorescence intensity was measured. The baseline

blood and ISF glucose level of rats were measured by glucometer and RFMID, respectively. Subsequently, 4 units of insulin were injected to the rats subcutaneously and blood glucose levels were tracked by glucometer every 5 min. The RFMID patches were applied on rats' skin and fixed with Tegaderm tape for 5 min, when blood glucose level decreased to certain ranges (5 ranges in total): T0: 25 – 35 mM, T1: 15 – 25 mM, T2: 10 – 15 mM, T3: 5 – 10 mM, T4: 3 – 5 mM. After reaching to hypoglycemia regime, 0.5 mL of 30% glucose solution was intraperitoneally injected into the rats, followed by another two time-point ISF glucose measurements by RFMID. After drying at room temperature, RFMID patches were observed under the microscope and their fluorescence intensity was recorded. For each timepoint, at least three RFMID patches were applied, and the average fluorescence intensity was reported as the RFMID measurement. Rats' ISF glucose levels were calculated by interpolating the fluorescence intensity difference before and after detection into the *ex vivo* RFMID glucose detection calibration curve.
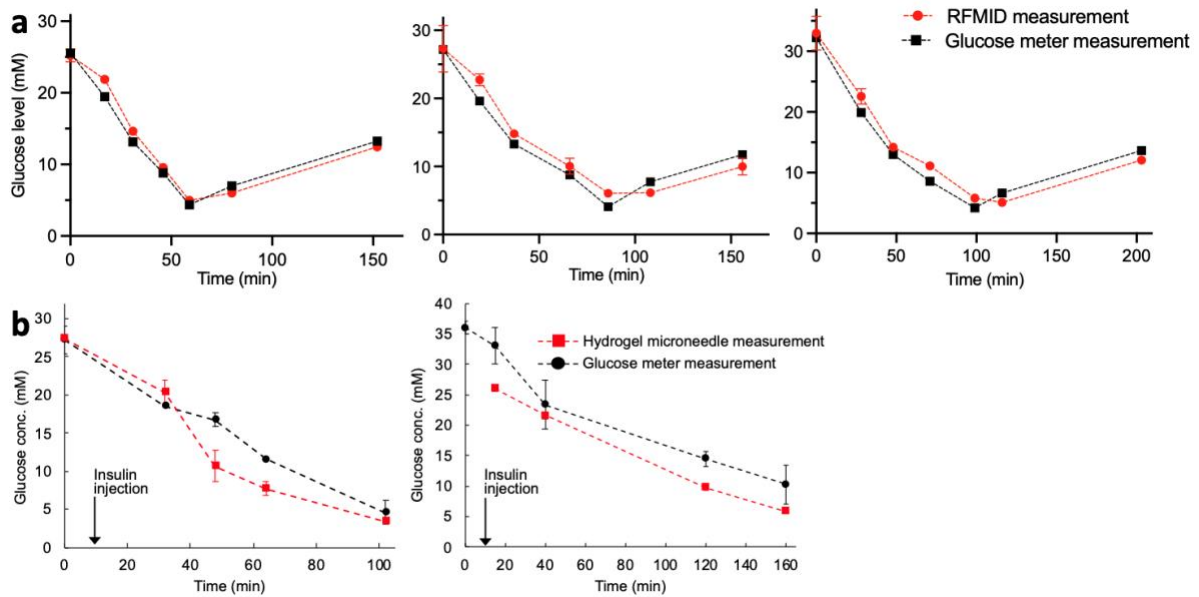
Figure 4.4 RFMID measurement of glucose levels in three different diabetic rats over 150-200 mins. The rats were injected with 4 IU kg−1 dose of human recombinant insulin (at t = 5 min; after baseline measurement) subcutaneously or 30% glucose solution (at t = 63, 93, 109 min for different rats and after reaching hypoglycemia condition) intraperitoneally to reduce or increase the blood glucose level, respectively. After reaching each range, the RFMID patches were applied to the dorsal skin of rats for 5 mins. Data is expressed as mean ± s.d. n = 3 replications per group.

The RFMID patches for glucose detection were applied at different time points and kept on the skin for 5 min (Figure 4.4 a&b). These results demonstrate that the RFMID device can track the falling and rising glucose concentrations in animal models. In parallel, we compared the RFMID results with conventional glucose measurements from a handheld glucose meter using blood samples collected from the rat tail vein and observed that both sets of results correlated well with a time lag of 3-14 mins. This time lag is attributed to the locations of glucose and differing transport efficiencies between ISF and circulating blood. Patients with diabetes also showed a time lag of 4–10 min in the change of ISF glucose levels relative to blood glucose concentrations[65]. The differences between glucose responses in individual rats clearly show the inter-individual variability, even under controlled conditions with genetically similar animals. This has important implications for human patients, who are genetically diverse and exposed to different environmental conditions. Thus, these results highlight the necessity of personalized glucose monitoring using a simple and reagentless approach.

Chapter 5

Conclusion

Herein, we demonstrated the first technology to combine HMN arrays with aptamer probes to summon their merits for reagentless and minimally invasive target detection. We showed a comprehensive characterization of our HMN patches functionalized with aptamer probes where addition of the aptamer probes did not have a significant effect on the swelling ability or mechanical strength of the patches. Experiments in skin specimens equilibrated with varying concentrations of target analytes indicate that our sensor has high sensitivity and specificity to detect clinically relevant concentrations of a wide range of analytes, with a LOD of 1.1 mM for glucose, 0.1 mM for ATP, 3.5 µM for L-tyrosinamide, and 25 nM for thrombin. The RFMID assay's response time to capture and detect the target analytes is only 2 min because of the swelling capabilities of MeHA that enable rapid ISF access and the reagentless detection mechanism. This fast response time is an exceptional improvement over previously reported MN-based diagnostic devices (Table 3.1). The patches can be stored at the room temperature for 14 days with no significant decrease on the assay response. *In vivo* experiments in awake diabetic rats confirmed the RFMID ability to measure changes in glucose with no need for adding any reagents and highlighted the RFMID platform's capacity to detect inter-individual variations in glucose response between animals - a critical feature for clinical implementation. Importantly, RFMID measurements closely matched those obtained with standard clinical glucose meters. Table 5.1 compared the RFMID performance for glucose measurement with the current state-of-the-art transdermal biosensing technologies, demonstrating that the assay can be reliably used for glucose measurement while the capability of other biomarker analysis is on the horizon of our assay to complement glucose measurement.

Table 5.1 The comparison of RFMID performance with the current state-of-the-art of transdermal biosensors.

Recent report on transdermal biosensors	Technique/in-vivo or ex-vivo measurement	Response time	LOD	Dynamic range	Long-term stability/ storage	Implanted lifetime	Generaliz-ability
Dexcom G6[27]	Transdermal glucose sensing /*in vivo*-human	2 hr warm-up time	2.2 mM	2.2 mM-22.2 mM	3 months (sensor)	10 days	No
Enlite Sensor (Guardian REAL-Time System)[28]	Transdermal glucose sensing /*in vivo*-human	2 hr warm-up time	2.2 mM	2.2 mM-22.2 mM	1 year (transmitter)	7 days	No
Abbott FreeStyle Libre[29]	Amperometry electrochemical sensor/*in vivo*-human	1 hr warm-up time	2.2 mM	2.2 mM-27.8 mM	3 years (transmitter)	14 days	No
Ref [26]	Glucose sensor integrated with HMN patch/*ex vivo*	3 min	10 µM	10 µM-16 mM	-	-	No
Ref [17]	Off-site glucose detection using glucose kits/*in vivo*	> 80 min	-	2.8 mM-33 mM	-	-	Yes
RFMID	Aptamer probes integrated with HMN patch/*in vivo*	2 min	1.1 mM	3.5 mM-32 mM	14 days	-	Yes

Although it is beyond the scope of this work, we believe our system could be modified for continuous, real-time measurement in a minimally invasive manner. The linkage of the quencher strand into the aptamer probe via a PEG linker (the technique used for thrombin detection) averts the complete removal and release of the quencher strand upon target binding, thus enabling real-time and continuous measurement. In addition, miniaturized optical system using compact light-emitting devices and optical detection technologies such as photodetector can be fabricated and integrated with our system which has the potential of transforming the assay into a wearable platform[66]. With such modifications, an integrated technology to continuously collect individual patient molecular profiles in a minimally invasive manner can be deployed, allowing continuous and prolonged measurement of any targets of interest, such as drugs with narrow therapeutic range.

Finally, we emphasize that the RFMID system is a platform that could be readily modified to measure other circulating analytes *in vivo*, for which aptamer probes are available, thus making it potentially a versatile tool for diverse biomedical applications.

References

1. Vashist, S. K. *In vitro* diagnostic assays for COVID-19: Recent advances and emerging trends. *Diagnostics* **10**, (2020).
2. Vashist, S. K. Point-of-care diagnostics: Recent advances and trends. *Biosensors* **7**, 10–13 (2017).
3. Baird, G. Preanalytical considerations in blood gas analysis. *Biochem. Medica* **23**, 19–27 (2013).
4. Zhang, Y., Ma, C. B., Yang, M., Pothukuchy, A. & Du, Y. Point-of-care testing of various analytes by means of a one-step competitive displacement reaction and pregnancy test strips. *Sensors Actuators B Chem.* **288**, 163–170 (2019).
5. Li, Y., Uddayasankar, U., He, B., Wang, P. & Qin, L. Fast, Sensitive, and Quantitative Point-of-Care Platform for the Assessment of Drugs of Abuse in Urine, Serum, and Whole Blood. *Anal. Chem.* **89**, 8273–8281 (2017).
6. M.P., H., R.H., C., L.K., N., A.L., K. & E.M., O. Cardiac markers: Point of care testing. *Clin. Chim. Acta* **284**, 223–237 (1999).
7. Price, C. P. Regular review: Point of care testing. *Br. Med. J.* **322**, 1285–1288 (2001).
8. John, A. S. & P Price, C. Existing and Emerging Technologies for Point-of-Care Testing. *Clin. Biochem. Rev.* **35**, 155–167 (2014).
9. Hudson, M. P., Christenson, R. H., Newby, L. K., Kaplan, A. L. & Ohman, E. M. Cardiac markers: point of care testing. *Clin. Chim. Acta* **284**, 223–237 (1999).
10. IUPAC. Molecule. *IUPAC Compend. Chem. Terminol.* **1077**, 4002 (2008).
11. Goode, J. A., Rushworth, J. V. H. & Millner, P. A. Biosensor Regeneration: A Review of Common Techniques and Outcomes. *Langmuir* **31**, 6267–6276 (2015).
12. Ye, S., Feng, S., Huang, L. & Bian, S. Recent Progress in Wearable Biosensors: From Healthcare Monitoring to Sports Analytics. *Biosensors* **10**, 1–34 (2020).
13. Liu, G. S. *et al.* Microneedles for transdermal diagnostics: Recent advances and new horizons. *Biomaterials* **232**, 119740 (2020).
14. Kashaninejad, N., Munaz, A., Moghadas, H., Yadav, S. & Umer, M. *Microneedle Arrays for Sampling and Sensing Skin Interstitial Fluid*. (2021).
15. Samant, P. P. & Prausnitz, M. R. Mechanisms of sampling interstitial fluid from skin using a microneedle patch. *Proc. Natl. Acad. Sci. U. S. A.* **115**, 4583–4588 (2018).
16. Editor, S. & Wu, G. Y. *Chronic Liver Failure Mechanisms and Management*. (2004).
17. Zhu, J. *et al.* Gelatin Methacryloyl Microneedle Patches for Minimally Invasive Extraction of Skin Interstitial Fluid. *Small* **16**, 1–9 (2020).
18. Niedzwiecki, M. M. *et al.* Human Suction Blister Fluid Composition Determined Using High-Resolution Metabolomics. *Anal. Chem.* **90**, 3786–3792 (2018).
19. Miller, P. R. *et al.* Extraction and biomolecular analysis of dermal interstitial fluid collected with hollow microneedles. *Commun. Biol.* **1**, (2018).
20. Kiang, T. K. L., Häfeli, U. O. & Ensom, M. H. H. A comprehensive review on the pharmacokinetics of antibiotics in interstitial fluid spaces in humans: Implications on dosing and clinical pharmacokinetic monitoring. *Clin. Pharmacokinet.* **53**, 695–730 (2014).
21. Liu, G. S. *et al.* Microneedles for transdermal diagnostics: Recent advances and new horizons. *Biomaterials* **232**, 119740 (2020).
22. Kool, J. *et al.* Suction blister fluid as potential body fluid for biomarker proteins. *Proteomics* **7**, 3638–3650 (2007).
23. Samant, P. P. *et al.* Sampling interstitial fluid from human skin using a microneedle patch. *Sci. Transl. Med.* **12**, 1–16 (2020).

24. Chang, H. *et al.* A Swellable Microneedle Patch to Rapidly Extract Skin Interstitial Fluid for Timely Metabolic Analysis. *Adv. Mater.* **29**, 1–8 (2017).
25. Zhang, X., Chen, G., Bian, F., Cai, L. & Zhao, Y. Encoded Microneedle Arrays for Detection of Skin Interstitial Fluid Biomarkers. *Adv. Mater.* **31**, 1–8 (2019).
26. Zheng, M. *et al.* Osmosis-Powered Hydrogel Microneedles for Microliters of Skin Interstitial Fluid Extraction within Minutes. *Adv. Healthc. Mater.* **9**, 1–11 (2020).
27. Dexcom. Using Your Dexcom G6 Guide.
28. Medtronic. Enlite Sensor (Guardian REAL-Time System) User Guide.
29. Abbott. Abbott FreeStyle Libre User Guide. (2022).
30. Rainer Hofmann-Wellenhof GiovanniPellacani. *Reflectance Confocal Microscopy for Skin Diseases*. (2546).
31. Serrano-Castañeda, P., Escobar-Chávez, J. J., Rodríguez-Cruz, I. M., Melgoza-Contreras, L. M. & Martínez-Hernández, J. Microneedles as enhancer of drug absorption through the skin and applications in medicine and cosmetology. *J. Pharm. Pharm. Sci.* **21**, 73–93 (2018).
32. Li, J. *et al.* Fabrication of gradient porous microneedle array by modified hot embossing for transdermal drug delivery. *Mater. Sci. Eng. C* **96**, 576–582 (2019).
33. Yi, K. *et al.* Aptamer-decorated porous microneedles arrays for extraction and detection of skin interstitial fluid biomarkers. *Biosens. Bioelectron.* **190**, (2021).
34. Poldervaart, M. T. *et al.* 3D bioprinting of methacrylated hyaluronic acid (MeHA) hydrogel with intrinsic osteogenicity. *PLoS One* **12**, 1–15 (2017).
35. Wiraja, C., Ning, X., Cui, M. & Xu, C. Hydrogel-Based Technologies for the Diagnosis of Skin Pathology. *Technologies* **8**, 47 (2020).
36. Tejavibulya, N. *et al.* Hydrogel Microfilaments toward Intradermal Health Monitoring. *iScience* **21**, 328–340 (2019).
37. Romanyuk, A. V. *et al.* Collection of analytes from microneedle patches. *Anal. Chem.* **86**, 10520–10523 (2014).
38. He, R. *et al.* A Hydrogel Microneedle Patch for Point-of-Care Testing Based on Skin Interstitial Fluid. *Adv. Healthc. Mater.* **9**, 1–11 (2020).
39. Laszlo, E., De Crescenzo, G., Nieto-Argüello, A., Banquy, X. & Brambilla, D. Superswelling Microneedle Arrays for Dermal Interstitial Fluid (Prote)Omics. *Adv. Funct. Mater.* **31**, 1–14 (2021).
40. Kim, J., Campbell, A. S., de Ávila, B. E. F. & Wang, J. Wearable biosensors for healthcare monitoring. *Nat. Biotechnol.* **37**, 389–406 (2019).
41. Teymourian, H. *et al.* Microneedle-Based Detection of Ketone Bodies along with Glucose and Lactate: Toward Real-Time Continuous Interstitial Fluid Monitoring of Diabetic Ketosis and Ketoacidosis. *Anal. Chem.* **92**, 2291–2300 (2020).
42. Goud, K. Y. *et al.* Wearable Electrochemical Microneedle Sensor for Continuous Monitoring of Levodopa: Toward Parkinson Management. *ACS Sensors* **4**, 2196–2204 (2019).
43. Wang, Z. *et al.* Microneedle patch for the ultrasensitive quantification of protein biomarkers in interstitial fluid. *Nat. Biomed. Eng.* **5**, 64–76 (2021).
44. Tang, Z. *et al.* Aptamer switch probe based on intramolecular displacement. *J. Am. Chem. Soc.* **130**, 11268–11269 (2008).
45. Munzar, J. D., Ng, A. & Juncker, D. Duplexed aptamers: History, design, theory, and application to biosensing. *Chem. Soc. Rev.* **48**, 1390–1419 (2019).
46. FDA. Approved Dermal Fillers. (2020).
47. Ye, Y. *et al.* Microneedles Integrated with Pancreatic Cells and Synthetic Glucose-Signal Amplifiers for Smart Insulin Delivery. *Adv. Mater.* **28**, 3115–3121 (2016).
48. Vianini, E., Palumbo, M. & Gatto, B. *In vitro* selection of DNA aptamers that bind L-tyrosinamide. *Bioorganic Med. Chem.* **9**, 2543–2548 (2001).

49. Mohorko, N., Petelin, A., Jurdana, M., Biolo, G. & Jenko-Pražnikar, Z. Elevated serum levels of cysteine and tyrosine: Early biomarkers in asymptomatic adults at increased risk of developing metabolic syndrome. *Biomed Res. Int.* **2015**, (2015).

50. Zhang, Y. *et al.* Thrombin-Responsive Transcutaneous Patch for Auto-Anticoagulant Regulation. *Adv. Mater.* **29**, 1–7 (2017).

51. Papakonstantinou, E., Roth, M. & Karakiulakis, G. Hyaluronic acid: A key molecule in skin aging. *Dermatoendocrinol.* **4**, 253–258 (2012).

52. Waghule, T. *et al.* Microneedles: A smart approach and increasing potential for transdermal drug delivery system. *Biomed. Pharmacother.* **109**, 1249–1258 (2019).

53. Guo, J., Zhang, H., Li, C., Zang, L. & Luo, J. In situ synthesis of poly(methyl methacrylate)/SiO 2 hybrid nanocomposites via grafting onto strategy based on UV irradiation in the presence of iron aqueous solution. *J. Nanomater.* **2012**, (2012).

54. Bencherif, S. A. *et al.* Influence of the degree of methacrylation on hyaluronic acid hydrogels properties. *Biomaterials* **29**, 1739–1749 (2008).

55. Alkhamis, O., Canoura, J., Yu, H., Liu, Y. & Xiao, Y. Innovative engineering and sensing strategies for aptamer- based small-molecule detection. *Trends Anal. Chem.* **121**, (2019).

56. Il'icheva, I. A., Nechipurenko, D. Y. & Grokhovsky, S. L. Ultrasonic cleavage of nicked dna. *J. Biomol. Struct. Dyn.* **27**, 391–397 (2009).

57. Nakatsuka, N. *et al.* Aptamer-field-effect transistors overcome Debye length limitations for small-molecule sensing. *Science (80-.).* **362**, 319–324 (2019).

58. Poudineh, M. *et al.* A fluorescence sandwich immunoassay for the real-time continuous detection of glucose and insulin in live animals. *Nat. Biomed. Eng.* **5**, 53–63 (2021).

59. Wilson, B. D., Hariri, A. A., Thompson, I. A. P., Eisenstein, M. & Soh, H. T. Independent control of the thermodynamic and kinetic properties of aptamer switches. *Nat. Commun.* **10**, 1–9 (2019).

60. Feagin, T. A., Olsen, D. P. V., Headman, Z. C. & Heemstra, J. M. High-throughput enantiopurity analysis using enantiomeric DNA-based sensors. *J. Am. Chem. Soc.* **137**, 4198–4206 (2015).

61. Laffel, L. Ketone bodies: A review of physiology, pathophysiology and application of monitoring to diabetes. *Diabetes. Metab. Res. Rev.* **15**, 412–426 (1999).

62. Dungan, K. & Verma, N. Monitoring Technologies – Continuous Glucose Monitoring, Mobile Technology, Biomarkers of Glycemic Control. *Endotext* (2000).

63. Chen, Y. C. *et al.* Functional human vascular network generated in photocrosslinkable gelatin methacrylate hydrogels. *Adv. Funct. Mater.* **22**, 2027–2039 (2012).

64. Yu, J. *et al.* Glucose-responsive insulin patch for the regulation of blood glucose in mice and minipigs. *Nat. Biomed. Eng.* **4**, 499–506 (2020).

65. Boyne, M. S., Silver, D. M., Kaplan, J. & Saudek, C. D. Timing of Changes in Interstitial and Venous Blood Glucose Measured with a Continuous Subcutaneous Glucose Sensor. *Diabetes* **52**, 2790–2794 (2003).

66. Dhanabalan, S. S. *et al.* Wearable Label-Free Optical Biodetectors: Progress and Perspectives. *Adv. Photonics Res.* **2**, 2000076 (2021).

Appendix A

Table A1 Sequence and modification of aptamer probe and competitor strands

Name	5' mod	Internal mod	3' mod	Sequence (5' to 3')
Glucose aptamer	5Acryd	iCy3		CTCTCGGGACGACCGTGTGTGTT GCTCTGTAACAGTGTCCATTGTCG TCCC
Glucose competitor			3Dab	GGTCGTCCCGAGAG
ATP aptamer	5Acryd	iCy3		CACCTGGGGGAGTATTGCGGAGG AAGG
ATP competitor			3Dab	TTTTCCAGGTG
L-tyrosinamide aptamer	5Acryd	iCy3		GGAGCTTGGATTGATGTGGTGTG TGAGTGCGGTGCCC
L-tyrosinamide competitor			3Dab	TCACATCAAT
Thrombin aptamer-competitor complex	5Acryd	iCy3 isp18	3Dab	CCAAC $(CH_2CH_2O)_{30}$GGTTGGTGTGGTTGG
Thrombin aptamer	5Acryd	iCy3		GGTTGGTGTGGTTGG
Thrombin competitor			3Dab	TTTTTCAACC

Appendix B

Statistical analysis

All the statistical analysis was conducted using GraphPad Prism 9. The statistical difference between groups in biocompatibility test, RFMID specificity test and swelling experiment was analyzed using ordinary one-way ANOVA with Tukey's multiple comparison test. In glucose recovery experiment, the statistical difference between different HMN groups and various glucose concentrations were analyzed using two-way ANOVA with Geisser-Greenhouse correction. The significance of statical difference was calculated with 95% confidence interval ($P<0.05$) and shown in GP style (0.1234 (ns), 0.0332 (*), 0.0021 (**), 0.0002 (***), <0.0001 (****)) in graphs. Each experiment contains three parallel replicates. All data is expressed as mean ± s.d. For *in vitro* and *ex vivo* glucose and ATP measurement, fluorescence signal raw data after subtracting the background signal was used to calculate the calibration curves using the sigmoidal 4PL nonlinear regression model. The LOD is defined as the minimum target concentration that can be detected by our RFMID device and calculated by interpolating the mean fluorescence signal of control group plus three times of s.d. into the corresponding calibration curve[45].